The Famenin fall and other ordinary chondrites intermediate between H and L groups

Hamed Pourkhorsandi, J. Gattacceca, Pierre Rochette, Thomas Smith, Lydie Bonal, Massimo D'orazio, Bertrand Devouard, Corinne Sonzogni, Vinciane Debaille

Title: The Famenin fall and other ordinary chondrites intermediate between H and L groups

Authors: Hamed Pourkhorsandi✉[1, 2], Jérôme Gattacceca[1], Pierre Rochette[1], Thomas Smith[3], Lydie Bonal[4], Massimo D'Orazio[5], Bertrand Devouard[1], Corinne Sonzogni[1], Vinciane Debaille[2]

[1]Aix-Marseille Univ, CNRS, IRD, INRAE, CEREGE, Aix-en-Provence, France

[2]Laboratoire G-Time, Université Libre de Bruxelles, CP 160/02, 50, Av. F.D. Roosevelt, 1050 Brussels, Belgium

[3]Institute of Geology and Geophysics, Chinese Academy of Sciences, 19 Beitucheng Western Road Chaoyang District, Box 9825 Beijing, 100029, China

[4]Institut de Planétologie et d'Astrophysique de Grenoble, Grenoble, France

[5]Dipartimento di Scienze della Terra, Università di Pisa, Pisa, Italy

✉Corresponding author. E-mail address: hamed.pourkhorsandi@ulb.ac.be

Revision to be submitted to the *Meteoritics and Planetary Science (MAPS)*

Last update: 16/12/2021

Abstract

The Famenin meteorite fell around 08:30 am local time (GMT+4.5) on 27 June 2015 on the roof of a house in Famenin town, NW Iran. A single 640 grams stone was recovered, shattered into several pieces upon impact. The shape of the impact hole and the relative position of the recovered meteorites indicate a N-NW fall direction. Famenin is an ordinary chondrite with well preserved chondrules of various types, (Fe,Ni) metal, troilite, phosphate, and chromite. The organic matter systematics and the olivine and low-Ca compositional distributions (percent mean deviations 18% and 31%, respectively) indicate it is a type 3.4/3.8 chondrite. Considering the average chemical compositions of olivine ($Fa_{17.5\pm4.7}$) and low-Ca pyroxene ($Fs_{16.8\pm7.5}$), average Co content of the kamacite (5.6 mgg^{-1}), and Cu/Ni and Ga/Ni ratios, Famenin should be classified as an H chondrite. However, saturation magnetization is 26.0 Am^2/kg, indicating a bulk metal content similar to L chondrites. Similarly, the whole rock Ni and Co contents (13073 and 540 μgg^{-1}, respectively), and average chondrule diameter (550 μm) are closer to typical values for L chondrites than H chondrites. The (Fe,Ni) metal modal abundance (5 vol%), magnetic susceptibility, and possibly whole rock oxygen isotopic composition indicate intermediate properties between H and L chondrites. Noble gas composition and cosmic ray exposure (CRE) ages of Famenin and El Médano 195 (another intermediate ordinary chondrite) shows their gas-rich character and an older ejection age from their parent body than those for the majority of H and L chondrites. Famenin, together with similar intermediate ordinary chondrites, increases the diversity of this meteorite clan and suggests the existence of a separate ordinary chondrite group with a composition broadly intermediate between H and L groups for which a different designation (HL) is proposed. Ordinary chondrites likely originate from more than three parent bodies (H, L, and LL) as traditionally proposed.

Keywords: Fall, Intermediate chondrite, HL, ordinary chondrites, classification

INTRODUCTION

Around 08:30 am local time (GMT+4.5) on 27 June 2015, a meteorite fell in Famenin town of Hamedan province (35° 7.12' N, 48°58.50' E) in Iran (Fig. S1). R. Salimi a resident of the town, heard the sound of an impacting object onto the roof of his house. He discovered that part of the roof was damaged and fragments of a stone were spread on the roof and in the yard. The impact had damaged the asphalt layer of the roof. Looking for the impactor, he found shattered fragments of the meteorite (Fig. 1). In addition, another sample (~ 10 grams) was found resting on the floor of the neighbor's house after breaking the window glass. The shape of the damaged roof and the relative position of the meteorite indicates a N-NW fall direction (Fig. 1a). News of the event propagated quickly via the local media. Despite additional searches by the locals, no additional samples were collected. No record of related fireball sighting or atmospheric detonation sounds were reported. Only two meteorite falls have been recorded in Iran before Famenin: Veramin mesosiderite(Graham and Hassanzadeh 1990; Ward 1901) and Naragh H6 chondrite (Adib and Liou 1979; Clarke 1975) fallen in 1880 and 1974, respectively.

The Famenin meteorite was classified at CEREGE (Aix-en-Provence) as H/L3 (i.e. an ordinary chondrite with intermediate properties between those of the H and L groups) and published in the Meteoritical Bulletin (Bouvier et al. 2017). Ordinary chondrites (OCs) with such intermediate characteristics are rare, and it has been suggested that they form an individual group (Kallemeyn et al. 1989; Trigo-Rodríguez et al. 2009; Wittmann et al. 2011). Tieschitz and Bremervörde are two H/L chondrites which have been investigated by other workers and proposed to be representative samples of this group.

As more work on new meteorites is being conducted, the meteorite classification scheme is developing. This is evidenced by recent works describing meteorites that do not belong to any of the recognized groups and that eventually form new groups (e.g., Weisberg et al. 2015; Pourkhorsandi et al. 2017; King et al. 2019; Metzler et al. 2021). These studies reveal a diversity of solar system materials higher than previously

assumed, mirroring the differences in physico-chemical conditions in the solar nebula and structures of meteorite parent bodies (Greenwood et al. 2020).

In this work, we investigate the petrography, mineral chemistry, whole rock trace element, oxygen isotopic compositions, noble gas composition, and physical properties of Famenin. In addition, in an effort to characterize intermediate H/L OCs and understand their relationships with H and L groups, we compare Famenin with Bremervörde (H/L3), El Médano 195 (EM 195, H/L3), Gursum (H5), Pavel (H3-anomalous), and San Juan 041 (SJ 041, H/L6).

METHODOLOGY

Three polished thin and thick sections of Famenin and thick sections of EM 195, Pavel, Gursum, and SJ 041 were prepared for petrographic studies. Mineralogical and petrological studies were conducted with a Leica DM2500P optical microscope and a Hitachi S3000-N Scanning Electron Microscope (SEM) equipped with a Bruker X-ray Energy Dispersive Spectrometer (EDS) at CEREGE. Chemical compositions of the mineral phases were determined with CAMECA SX50 and SX100 electron microprobes at the CAMPARIS facility (Paris). The operating conditions were focused electron beam (~ 1 µm in diameter), an accelerating voltage of 15 kV and a beam current of 10 nA. Both natural and synthetic standards were used for calibration: albite for Na; anorthite for Al; apatite for P; diopside for Mg, Si, Ca; orthoclase for K; pyrite for S; $MnTiO_3$ for Mn, Ti; Cr_2O_3 for Cr; Fe_2O_3 for Fe; NiO for Ni. For analyses of metallic phases, pure Ni, Fe and Co were used as standards. In addition to synthetic standards, we analyzed (Fe,Ni) metal in several H chondrites (Agen, Catalina 396, and Taqtaq-e Rasoul), L chondrites (Andila and Djadjarm), and LL chondrites (Bensour) (Table S1). The agreement between chemical composition (Fe, Co, and Ni) of kamacite in these chondrites with the ranges reported for their corresponding groups was used to check the accuracy of our metal analysis. It should be noted that the measurement spots were chosen randomly including both the core and rims of grains aiming to analyze areas with diverse chemical compositions.

Magnetic measurements were performed at CEREGE. Magnetic susceptibility was measured using a KLY2 instrument from Agico equipped with a large (65 cm^3) or a small (10 cm^3) coil. Magnetic hysteresis properties were measured with a Princeton Micromag vibrating sample magnetometer (VSM) with a noise level of about 1 nAm^2 and a maximum applied field of 1 T. Hysteresis loops allow the determination of coercivity (B_C), saturation magnetization (M_S), saturation remanent magnetization (M_{RS}), (χ_{HF}, including both diamagnetic and paramagnetic contributions). Coercivity of remanence (B_{CR}) was evaluated through DC back-field demagnetization of the saturation remanence.

The whole rock trace element content of Famenin was determined by Inductively Coupled Plasma - Mass Spectrometry (ICP-MS) using a Perkin-Elmer NexION® 300x spectrometer at the Pisa University's Dipartimento di Scienze della Terra. Allende carbonaceous chondrite reference sample (USNM 3529, split 20, position 22) was dissolved and analyzed along with Famenin to check the accuracy of the results. About 50-100 mg of each powder were dissolved in a mixture of HF and HNO_3 on a hot plate at ~120 °C inside screw-top perfluoroalkoxy (PFA) vessels. Then the sample solutions were diluted to 50 mL in polypropylene vials. In each step of sample preparation, Mill-Q® purified water (18.2 M cm), ultrapure HF and HNO_3 were used. The sample solutions were introduced into the plasma after online mixing with a solution containing 20 ng/mL each of Rh, Re and Bi as internal standards. The elements Li, Be, Ni, Co, Ga, Rb, Sr, Y, Zr, Nb, , Cs, Ba, REE, Hf, Ta, W, Pb, Th, U were determined in "standard mode", whereas the elements Sc, Cu, Zn were determined in "kinetic energy discrimination mode, KED" using a He flow of 3.7 mL/min. Analyses were done using an external calibration performed with a solution of the BE-N (alkaline basalt) geochemical reference sample. In Table 1 the results of the ICP-MS analyses of Allende along with the literature values are reported. The analytical precision is between 5 and 10% RSD for elements with concentrations > 0.5 µg/g and between 10 and 20% RSD for elements with concentrations < 0.5 µg/g.

Measurements of $\delta^{18}O$ and $\delta^{17}O$ of two Famenin 1.5 mg aliquot of silicates hand-picked from a powdered and acid-washed 200 mg bulk sample were carried out at the

Stable Isotopes Laboratory of CEREGE. Laser fluorination coupled with isotope ratio mass spectrometry (IRMS) (Alexandre et al., 2006; Crespin et al., 2008) adapted for measurement of extraterrestrial materials (Suavet et al. 2010) was used for this purpose. The three oxygen isotopic compositions were measured with a dual-inlet mass spectrometer Thermo-Finnigan Delta Plus. In addition to Famenin, we analyzed 1.5 mg samples of Bremervörde (H/L3), EM 195 (H/L3), Gursum (H5), Pavel (H3-anomalous), SJ 041 (H/L6) as well as Ochansk (H4), Paranaiba (L6), and Homestead (L5), as example of regular ordinary chondrites. The initial bulk sample was powdered, sieved between 100 and 400 µm, cleaned with 1M HCl at 50°C for several hours to remove metal and sulfides, and rinsed with ethanol. Additional leaching with mono-ethanolamine-thioglycolate (EATG) was performed for weathered finds, to remove oxyhydroxides formed during weathering on Earth (see Greenwood et al. 2017 for the use of EATG in this context). The average mass of the initial bulk samples was 73 mg, ensuring that the 1.5 mg aliquot is representative of the bulk oxygen isotopic composition. The oxygen isotope results are expressed in ‰ versus the international reference standard V-SMOW: $\delta^{18}O = [(^{18}O/^{16}O)_{sample}/(^{18}O/^{16}O)_{V\text{-}SMOW}\text{-}1]\times1000$ and $\delta^{17}O = [(^{17}O/^{16}O)_{sample}/(^{17}O/^{16}O)_{V\text{-}SMOW}\text{-}1]\times1000$. The $\delta^{18}O$ and $\delta^{17}O$ values of the reference gas were calibrated with measurements of NBS28 standard ($\delta^{18}O$=9.60‰, Gröning, 2004). $\Delta^{17}O$ is computed as $\Delta^{17}O = \delta^{17}O - 0.52 \times \delta^{18}O$. The $\delta^{17}O$ value of the NBS28 standard ($\delta\ ^{17}O$ = 4.992‰) was computed so as to give $\Delta^{17}O$=0‰. The measurements were corrected on a daily basis using 1.5 mg quartz internal laboratory standard “Boulangé” (Alexandre et al. 2006; Suavet et al. 2010). During the analyzing period, the analytical uncertainties (1σ) derived from repeated measurement (n= 7) of this internal laboratory standard are 0.10‰, 0.16‰, 0.02‰ for $\delta\ ^{17}O$, $\delta\ ^{18}O$ and $\Delta^{17}O$, respectively.

The Raman spectroscopy was performed at Laboratoire de Géologie de Lyon Terre, Planètes, Environnement (ENS Lyon) with a Labram spectrometer (Horiba-Jobin-Yvon) equipped with a Spectra Physics Argon ion laser and using 514.5 nm excitation. Carbonaceous matter is sensitive to laser-induced heating and can be locally altered. Moreover, the Raman bands of the polyaromatic carbonaceous matter are dispersive. Thus, to avoid any laser alteration of the carbonaceous matter and to have a meaningful comparison with reference meteorites from the literature, the same experimental and

analytical conditions as in Bonal et al. (2016) were used. Raman spectra of the carbonaceous matter in Famenin were obtained both on isolated matrix grains and in-situ in a polished section. A raw piece of approximately 200 mg was gently crushed. Around 30 matrix fragments (typical apparent diameter around 30 μm) were then manually selected according to their color and texture under a binocular microscope. The selected matrix fragments were pressed between two glass slides that were also used as substrate for the Raman analysis. This procedure allows working on ‘‘fresh” samples and helps enhance heat dissipation, thereby minimizing thermal damage. Measurements made over two different sessions on two aliquots provided similar results.

Gamma spectroscopy and intensity measurements of ^{7}Be, ^{54}Mn, ^{22}Na, and ^{26}Al of the two larger fragments (total ~23 g) were carried out from 16 to 24 July 2015 (683500 seconds) in LSCE (Gif-sur-Yvette, France).

The noble gas concentrations and isotopic ratios (^{3,4}He, ^{20,21,22}Ne, and ^{36,38,40}Ar) of EM 195, SJ 041, and Famenin were measured using a Noblesse (Nu) multi-collector noble gas mass spectrometer in the noble gas laboratory at the Institute of Geology and Geophysics, Chinese Academy of Sciences, Beijing, China. The analytical approach follows the same procedures as described in Ranjith et al. (2017). Briefly, samples with masses ranging from ~3 to ~5 mg were first washed with ethanol in an ultrasonic bath, weighed, and then loaded into the laser sample chamber of the noble gas extraction and purification line. The He standard is the “He Standard of Japan” (“HESJ”), with a calibrated ^{3}He/^{4}He ratio of 20.6±0.1 Ra (Matsuda et al. 2002), where Ra stands for the ^{3}He/^{4}He ratio of air (i.e. 1.4×10^{-6}). The average sensitivities for ^{4}He, ^{22}Ne, and ^{36}Ar are, in units of cm^{3}STP/counts, 3.67×10^{-15}, 3.17×10^{-15}, and 4.26×10^{-16}, respectively. Blanks were frequently measured using the exact same procedure as for the samples (see details below). They contribute for less than 1% for He, less than 2% for Ne, and less than 5% for Ar isotopes. Noble gases have been extracted by heating the samples in a single extraction step, using a CO_2 laser (1.064 μm wavelength, 3 mm diameter) for ~30 minutes. The released gases were cleaned from all reactive gases such as hydrocarbons, etc. using a series of getters, operating at room temperature and 200°C (Ranjith et al. 2017). The He-Ne fraction is separated from the Ar fraction using an activated charcoal held at the temperature of liquid nitrogen (LN_2) for 20 minutes.

Subsequently, the Ne is separated from the remaining He by using a cryogenic cold trap at 35K for 10 minutes. A fraction of the He gas is then inlet into the mass spectrometer. The Ne fraction is released at 80K for 30 minutes and the total gas fraction is inlet into the mass spectrometer; remaining background gases, such as hydrocarbons and Ar, which would compromise the Ne measurements, are further reduced using a charcoal held at LN_2 temperature during the Ne measurements. Finally, Ar is released at ~150°C for 20 minutes, and a known fraction of the gas is measured.

RESULTS

Macroscopic description

Upon the impact on the ground, the Famenin meteorite fragmented into two large and eight small pieces. The total recovered mass is 630 g. The two larger pieces total 565 g while the smaller fragments have masses between 5 and 25 g (Fig. 1). Famenin has weakly developed regmaglypts and the fusion crust has a black to dark-brown color with shiny patches of glassy material covering the fusion crust as an additional layer. The remnants of roofing asphalt material can be seen as black patches with sizes up to 5 cm.

The meteorite broken surface reveals a light grey interior. Distinct chondrules, (Fe,Ni) metal and troilite are easily discernible with the naked eye. (Fe,Ni) metal grains show no sign of weathering. A few fine-grained mm to cm-sized clasts with light lithology are also visible (Fig. 1b), although they were not present in the studied type specimen.

Optical and electron microscopy

Famenin

The fusion crust shows a vesicular texture with magnetite grains in the outermost layer and thin troilite veinlets formed by melting and recrystallization of the primary troilite during atmospheric passage of the meteoroid (Fig. 2, 3a). Point counting of a ~ 10 cm^2 surface under reflected light optical microscopy, with a step-size of 50 μm, yields the following proportions: 90.0 vol% silicates, 5.0 vol% (Fe,Ni) metal, and 5.0 vol%

troilite (n = 584). Barred olivine, cryptocrystalline, porphyritic, and radial pyroxene chondrule types are present (Fig. 2, 3). The average apparent chondrule diameter is 550 ± 296 µm (1σ; n = 100), with a median, mode, and maximum diameters of 510, 360, and 1960 µm, respectively (Fig. 4). Backscattered electron (BSE) images of the Famenin chondrite are shown in Fig. 3b-g. Olivine and pyroxene are not completely equilibrated and show a normal zoning with higher Fe (and lower Mg) in mineral rims than in mineral cores. Overall, olivine is more homogeneous than pyroxene. The matrix is mostly clastic and comprises individual (Fe,Mg) silicates and chondrule fragments. (Fe,Ni) metal and troilite are not completely separated from each other. Compared to troilite, most of the (Fe,Ni) metal grains are relatively rounded. Opaque rims consisting mostly of troilite aggregated with (Fe,Ni) metal and (Fe,Mg) silicates surround some of the chondrules. Fig. 3-g shows a barred olivine chondrule with normal zoning containing dendritic clinopyroxene crystallized out of the felsic mesostasis. Olivine exhibits undulatory extinction and displays planar fractures with about 200 µm spacing. Troilite displays finely polycrystalline textures with domain size of about 10 µm (Fig. 3h).

El Médano 195

EM 195 is a find classified as H/L3 (Ruzicka et al. 2015). A mosaic image is shown in Fig. S2. Point counting of a ~ 1.2 cm^2 surface under reflected light optical microscopy, with a step-size of 80 µm, yields the following proportions: 79.0 vol% silicates, 9.0 vol% (Fe,Ni) metal, and 12.0 vol% troilite (n = 531). Most (Fe,Ni) metal and troilite grains are in contact with each other. Troilite rims around chondrules are preserved and few (Fe,Ni) metal globules are present. Average apparent chondrule diameter is 570 ± 331 µm (1σ; n = 84), with a median, mode, and maximum diameters of 480, 426, and 1970 µm, respectively (Fig. 4). The abundance of the weathering products is low with only thin rims of Fe oxides/oxyhydroxides around few (Fe,Ni) metal grains, indicating a weathering grade W1 (Wlotzka 1993).

San Juan 041

SJ 041 is a find classified as H/L6 (Garvie 2012). Thermal metamorphism has led to the recrystallization of chondrules and the separation of (Fe,Ni) metal and troilite from each other (Fig. S3). Elongation of the (Fe,Ni) metal and troilite and the presence of

melt pockets containing troilite droplets indicates that SJ 041 is heavily shocked. Point counting under reflected light optical microscopy, with a step-size of 80 µm, yields the following proportions: 84 vol% silicates, 7 vol% (Fe,Ni) metal, and 8 vol% troilite (n = 601). The meteorite has a weathering grade W2.

Pavel

Pavel is a fall, classified as a H5. However, Dekov et al. (2017) proposed reclassification as H3-anomalous. The thick section used in present study is the same as used by Dekov et al. (2017). A mosaic image is shown in Fig. S4. Pavel has a well-defined chondrules with average apparent diameter of 485 ± 186 µm (1σ; n = 33) in agreement with measurements by Dekov et al. (2017), with a median, mode, and maximum diameters of 440, 400, and 840 µm. (Fe,Ni) metal and troilite grains are devoid of any alteration evidences (weathering grade W0).

Mineral chemistry

The representative chemical compositions of olivine, low-Ca pyroxenes, and (Fe,Ni) metal in Famenin are reported in Table 2 and 3. Low-Ca pyroxenes show a wider composition range than the olivine (Fs0.7-36.6 vs. Fa5.9-30.9) (Fig. 5). The percent mean deviations (PMD) are 31% and 18% for low-Ca pyroxene and olivine, respectively. Average olivine and low-Ca pyroxene compositions are $Fa_{17.5\pm4.7}$ (n = 71) and $Fs_{16.8\pm7.5}Wo_{4.3\pm5.9}$ (n = 35), respectively. The average Co concentration of kamacite is 4.7 ± 2.0 mg/g (n = 23, Table 3).

For EM 195, representative chemical compositions of olivine and low-Ca pyroxene are reported in Table 2. For EM 195, PMD for olivine and low-Ca pyroxene is 29% and 23%, respectively. The average Co concentration of kamacite is 3.8 ± 1.0 mg/g (n = 23, Table 3).

In accordance with the equilibrated texture, the mineral composition of olivine and low-Ca pyroxene of SJ 041 shows a narrow distribution (Table 2). PMD for olivine and low-Ca pyroxene is 0.8% and 3.5%, respectively. Average olivine and low-Ca pyroxene compositions are $Fa_{22.5\pm0.2}$ (n =4) and $Fs_{18.3\pm0.8}Wo_{1.1\pm0.9}$ (n = 5), respectively. The average Co content of kamacite is 5.9 ± 0.9 mg/g (n = 24).

Gursum an H4/5 (Graham 1983), later reclassified as an H5 by Schultz et al. (1990), has average olivine and low-Ca pyroxene compositions of $Fa_{16.0\pm0.3}$ (n =5) and $Fs_{14.2\pm0.2}Wo_{1.3\pm0.1}$ (n = 6), respectively (Table 2). Cobalt concentration of kamacite in this chondrite is 3.42 ± 1.1 mg/g (n = 24, Table 3).

Magnetic properties

The average magnetic susceptibility of Famenin measured on four pieces with masses in the range 5 - 11 grams is $\log\chi = 5.07 \pm 0.05$ (1σ) with χ in 10^{-9} m^3kg^{-1}. Saturation magnetization measured on a 80 mg fragment is $M_S = 24.9$ Am^2kg^{-1}. Hysteresis parameter ratios are $M_{RS}/M_S = 1.02x10^{-2}$ and $B_{CR}/B_C = 26.5$.

The magnetic susceptibilities of EM 195 (W1) and SJ 041 (W2) are $\log\chi = 4.99$ and $\log\chi = 4.59$, respectively.

Trace element bulk chemistry

The whole rock trace element composition of Famenin is reported in Table 1. CI-normalized spider diagrams of Famenin along with the mean values reported for H, L, and LL OCs (Wasson and Kallemeyn 1988) are shown in Fig. 6. Trace element content of Famenin is chondritic and it follows the general trend of OCs. Some highly volatile elements such as Rb, Li, Pb, and Ga in Famenin and OCs follow a similar enrichment and depletion patterns in relation to mean CI chondrites. However, Cs content in Famenin is closer to mean LL values than H and L chondrites. Lower concentrations of Ba and Be and higher Sr and Nb in Famenin compared to the OCs are other noticeable differences between them. Besides differences in absolute concentrations, deviations also exist in elemental ratios such as Sr/Ba which is 4.4, higher than the mean value for H (2.4), L (3.0), and LL (2.3) chondrites.

Oxygen isotopic composition

The whole rock oxygen isotopic composition analysis results for two aliquots of Famenin along with the data for other H, L, and intermediate ordinary chondrites that we analyzed are reported in the Table 4. Fig. 7 depicts the $\Delta^{17}O$ versus $\delta^{18}O$ values of Famenin along with the data for H, L, LL, and H/L chondrites. Literature data for

ordinary chondrites are compiled in Table 2S. Our test samples Homestead, Ochansk, and Paranaiba plot in the range of their respective chondrite groups. Our $\Delta^{17}O$ values of 1.00‰ and 0.97‰ (average 0.98‰) for Famenin, and 0.96‰ for Bremervörde, are in the very low range for L chondrites. They also show slightly higher $\delta^{18}O$ values than the majority of L chondrites and plot in the close vicinity of Tieschitz H/L chondrite (analyzed by Clayton and Mayeda 1991). SJ 041 with a $\Delta^{17}O$ of 1.02‰ with a higher $\delta^{18}O$ is also close to them. Pavel has a $\Delta^{17}O$ similar to H chondrites, however its $\delta^{18}O$ is more than one permil higher than most of them. EM 195 plots in the range of type 3 L chondrites. Officially classified as an H chondrite, Gursum has an oxygen isotopic composition similar to equilibrated L chondrites.

Organic matter

Each individual Raman spectra obtained on matrix of Famenin exhibits the D- and G-bands, attesting the presence of polyaromatic carbonaceous matter. Spectral differences (e.g., shape, relative intensity…) are visible on the raw Raman spectra, reflecting variable structural order of the polyaromatic carbonaceous matter within Famenin. These differences are confirmed by the range of spectral parameters obtained through the analytical adjustment. Spectral parameters of Famenin are variable but tend to be distributed among two main groups with the following mean values:

Famenin (A): $FWHM_D$ (cm^{-1}) = 151.8 ± 17.2 (n = 15) and I_D/I_G = 1.03 ± 0.06

Famenin (B): $FWHM_D$ (cm^{-1}) = 56.2 ± 13.6 (n = 15) and I_D/I_G = 1.13 ± 0.21

Spectra acquired on manually selected matrix grains are both of type “A” and “B”. However, this variability is not easily discernible in *in-situ* measurement data. Deciding whether the observed variability in bulk data results from brecciation is not possible based on available data.

Cosmogenic nuclides

Short-lived isotopes

The data show the presence of ^{7}Be ($t_{1/2}$ = ~ 53 days; 477 keV), ^{54}Mn ($t_{1/2}$ = ~ 312 days; 834.8 keV), ^{22}Na ($t_{1/2}$ = ~ 2.6 years; 1274.5 keV) and ^{26}Al ($t_{1/2}$ = 7.17×10^{5} years; 1808.65 keV). The detection of short-lived nuclides such as ^{7}Be and ^{54}Mn and the detailed reports in the media confirm the occurrence of this fall event.

Noble gas concentrations and isotopic ratios

The measured isotopic noble gas concentrations of the three chondrites corrected from interferences from $H2O^{+}$, $^{40}Ar^{++}$, and CO_2^{++} (on Ne isotopes) and for instrumental mass discrimination are presented in Table 5.

The cosmogenic Ne concentrations and isotopic ratios (index "cos") have been calculated and are reported in Table 6; To calculate the cosmogenic Ne concentrations and isotopic ratios in Famenin, we estimate Ne is a mixture between cosmogenic and SW endmembers ("SW" index). We assume $(^{20}Ne/^{22}Ne)_{SW}$=13.78±0.03 and $(^{21}Ne/^{22}Ne)_{SW}$=0.0329±0.0001 (Heber et al. 2009) as the SW endmember. To calculate the cosmogenic Ne concentrations and isotopic ratios in EM 195, we estimate a mixture between three endmembers: cosmogenic, SW, and air, the latter being characterized by $(^{20}Ne/^{22}Ne)_{air}$=9.80 and $(^{21}Ne/^{22}Ne)_{air}$=0.029. And $(^{20}Ne/^{22}Ne)_{cos}$=0.82 and $(^{21}Ne/^{22}Ne)_{cos}$=0.89 corresponding to the measured concentrations in SJ 041 (Fig. 8). The determined cosmogenic ratios $(^{22}Ne/^{21}Ne)_{cos}$ vary between 1.12 for SJ 041, and 1.95-2.52 for EM 195 and Famenin.

The measured $^{36}Ar/^{38}Ar$ and $^{40}Ar/^{36}Ar$ range from 3.96-5.04 and 90-535, respectively. In order to calculate the amount of cosmogenic $^{36}Ar_{cos}$ and $^{38}Ar_{cos}$, we used a three-component deconvolution assuming that the isotopic compositions are a mixture between cosmogenic, air, and SW endmembers. We used the following $(^{36}Ar/^{38}Ar)_{cos}$=0.63, $(^{36}Ar/^{38}Ar)_{air}$=5.32, and $(^{36}Ar/^{38}Ar)_{SW}$=5.47. The cosmogenic $^{36}Ar_{cos}$ and $^{38}Ar_{cos}$ concentrations are reported in Table 6.

Cosmic-ray exposure ages

The CRE ages (Table 7) have been calculated using the concentrations in cosmogenic $^{3}He_{cos}$, $^{21}Ne_{cos}$, and $^{38}Ar_{cos}$, later labelled T_3, T_{21}, and T_{38}, as described in e.g. Li et al. (2017) and using correlations given by (Eugster 1988). Based on these assumptions, CRE ages range from 4.99-8.71 Ma for SJ 041, with the common trend $T_3<T_{21}<T_{38}$, from 17.7-59.2 Ma for EM 195, and finally from 47.4-66.4 Ma for Famenin. Note that due to large discrepancies (most likely due to production rate calculation issues and/or He diffusive losses), we did not report the ^{3}He CRE ages T_3 for EM 195 and Famenin. In addition, for these two chondrites, we observe that the calculated T_{38} ages are systematically lower than T_{21}.

DISCUSSION

Classification of Famenin

Considering its mineralogy, bulk rock chemical composition, low abundance of matrix, and oxygen isotopic composition, Famenin is undoubtedly an ordinary chondrite, but it shares properties with both H and L chondrites, making its classification problematic. Its average chondrule size is closer to the value for L chondrites than for H chondrites (Metzler et al. 2018). On the other hand, average olivine and low-Ca pyroxene compositions are $Fa_{17.5\pm4.7}$ (n = 71) and $Fs_{16.8\pm7.5}Wo_{4.3\pm5.9}$ (n = 35), respectively, in the range of H chondrites values (Fig. 9) (Bearley and Jones, 1998). Oxygen isotopic bulk composition of Famenin is different from values measured in H chondrites (Fig. 7). Its $\Delta^{17}O$ is in the low range for L chondrites; however, $\delta^{18}O$ is higher in Famenin and is closer to the field of Tieschitz and Bremervörde H/L chondrites. The mean Co content in kamacite (4.7 mg/mg) is in the range of values reported for H chondrites (4.4-5.1 mg/g) (Fig. 10) (Afiattalab and Wasson 1980; Rubin 1990). The modal (Fe,Ni) metal abundance in Famenin is lower than the average H chondrite values (5 vol% versus 8 vol%) (Weisberg et al. 2006). Magnetic susceptibility χ and saturation magnetization (M_S) are other proxies to the bulk metal content, and can be used for the classification of meteorites (Rochette et al. 2003; Gattacceca et al. 2014). Magnetic susceptibility of Famenin ($\log\chi$ = 5.07) is intermediate between H (5.32 ± 0.10, n = 145 falls) and L chondrites (4.87 ± 0.10, n = 144 falls) , and similar to the magnetic susceptibility of Tieschitz (4.97) and Bremervörde (4.98) H/L chondrites (Rochette et al. 2003). Saturation magnetization of Famenin (M_S = 24.9 Am^2kg^{-1}) is in the range of values reported in Gattacceca et al. (2014) for L3 and L4 chondrites falls (22.1±5.1 Am^2kg^{-1}, N = 7) and much lower than the values for H3 and H4 falls (44.8±4.5 Am^2kg^{-1}, N = 8). Hysteresis parameter ratios are similar to the values observed in L and H chondrites, reflecting a combination of kamacite and taenite (Fig. S5). With a Ni content of 13.1 mg/g compared to the average values of H (16.0 mg/g), L (12.0 mg/g), and LL (10.2 mg/g) chondrites, Famenin is closer to the L chondrite range (Fig. 11a,b). Its bulk Co content is 540 µg/g, which compared to the average values of H (810 µg/g), L (590 µg/g) and LL (490 µg/g) chondrites, lies in between

L and LL chondrites (Wasson and Kallemeyn 1988) (Fig. 11b). Same applies for the Ga content (4.9 µg/g), in relation to mean H (6 µg/g), L (5.7 µg/g) and L (5 µg/g) chondrites (Fig. 6S) and as well as W which is closer to mean L chondrites (Fig. 6) However, when we consider the Cu/Ni and Ga/Ni ratios (Fig. 11c,d), which are known to increase from H to LL chondrites (Wasson and Kallemeyn 1988), Famenin falls in the range of H chondrites. Considering these evidences, we classify Famenin as a meteorite intermediate between H and L chondrites.

The observed Raman spectral parameters scatter reflects variable thermal metamorphism experienced by Famenin: type “A” spectra reflect thermal metamorphism comparable to that experienced by type 3.4 chondrites, while type “B” spectra reflect a higher thermal metamorphism (>3.7) (Fig. 12). It has to be noted that the type “A” spectra are internally quite variable as well, with spectral parameters of individual spectrum distributed over the metamorphic range observed in Bishunpur (3.1) to Tieschitz (3.6). This can be related to the structural grade of the polyaromatic carbonaceous matter which reveals variable degrees of thermal metamorphism in different parts of the meteorite. The PMD of olivine Fa content is 18%, indicating a petrologic type 3.8 (Sears et al. 1980),in broad agreement with data obtained by Raman spectroscopy (type “B” spectra). Based on these observations, we classify Famenin as a petrologic type 3 chondrite in the 3.4 to 3.8 range (Sears et al. 1980; 1982).

Based on the olivine optical microscopy, and using the classification of Stöffler et al. (2018), Famenin is very weakly shocked (S2 shock stage). However, random troilite polycrystalline texture in some parts (Fig. 3h) might suggest a higher shock degree (Ruzicka and Hugo 2018). Even though we did not study the two clasts visible in Fig. 1b in detail, but the macroscopic studies by us and (McCausland et al., 2016), heterogeneity observed in Raman spectroscopy data, and the noble gas compositions of Famenin favors its classification as a breccia. It should be mentioned that as the mentioned clasts are small relative to the bulk meteorite, in agreement with McCausland et al. (2016), we believe that they would not affect our main conclusions regarding Famenin’s intermediate properties.

Putting all these data together, we classify Famenin as an H/L3 (S2) brecciated chondrite.

Gas compositions

With a $^{20}Ne/^{22}Ne$ ratio of 0.82, we assume that Ne in SJ 041 is almost entirely cosmogenic (with $(^{20}Ne/^{22}Ne)_{cos}$ ~0.80, e.g., Leya et al., 2013). However, the measured $^{20}Ne/^{22}Ne$ ratios of 9.27 and 12.45 for EM 95 and Famenin, respectively, indicate that, in addition to cosmogenic noble gases, there is as well a contribution from a trapped component, here likely a solar wind (SW) contribution. The solar Ne isotopic ratios in meteorites are always distinct from the pure SW signature with $^{20}Ne/^{22}Ne = 13.7$ due to fractionation processes. The measured $^{21}Ne/^{22}Ne$ ratios vary between 0.097 - 0.19 for Famenin and EM 195, respectively. These data are in relatively good agreement with previous observations for other gas-rich meteorites, and consistent with a SW influence (Talahito and Keisuke 2006; Leya et al. 2009). The Ne three-isotope plot (Fig. 8) shows the Ne isotopic data (blank- and fractionation-corrected) for EM 195 and Famenin. The Ne isotopic ratios from SW, from solar cosmic-ray production (SCR-Ne), from galactic cosmic-ray production (GCR-Ne) and from air are also shown. From this plot, two important observations can be made. First, one can notice that the Ne isotopic composition of Famenin is a clear mixture between a cosmogenic component (here GCR-Ne) and SW; second, it appears the isotopic composition of EM 195 is a mixture between three components: cosmogenic, SW, and air. This is not surprising as EM 195 is a find which has been subjected to hot desert weathering and influenced by atmospheric contamination.

The range of $^{36}Ar/^{38}Ar$ ratios clearly indicate the presence of a trapped component, most likely atmospheric (SJ 041) and/or SW (presumably for EM 195 and Famenin). The composition of the bulk SW, measured by Genesis is $(^{36}Ar/^{38}Ar)_{SW} = 5.47\pm0.01$ (Heber et al. 2009); given the fact that only two Ar isotopes can be dominated by solar signature (i.e. $^{36,38}Ar$, ^{40}Ar is mainly radiogenic and dominated by decay of ^{40}K), an Ar three-isotope plot would not, unlike Ne, help to decipher the Ar endmember contributions (e.g. Rao et al. 1991).

Our gas data suggests that EM 195 and Famenin belong to a group of meteorites called “gas-rich” meteorites, i.e., meteorites that contain large amounts of primordial noble gases. Noble gas isotope records in gas-rich meteorites are explained by an

incorporation of gases produced by solar wind (SW) radiations (Suess et al. 1964), for a short period over few million years (Osawa and Nagao 2006). Gas-rich meteorites are as well characterized by $^{4}He \geq 10^{-4}$ cm^{3}STP/g (Megrue and Steinbrunn 1971). This is the case for Famenin, with ^{4}He concentration of 3.0×10^{-4} cm^{3}STP/g (see Table 5). The isotopic $^{4}He/^{3}He$ ratios for EM 195 and Famenin are 1503 and 3061, respectively. For comparison, the $(^{4}He/^{3}He)_{SW}$ is 2155 (Heber et al. 2009). However, the Solar Flare (SF) He obtained by Rao et al. (1991) is close to $(^{4}He/^{3}He)_{SF} = 3800 \pm 200$. We assume here that ^{3}He is entirely cosmogenic.

In Fig. 1b, one can observe the presence of mm to cm clasts, indicating that EM 195 (Fig. S2) and Famenin are breccias. In addition, as mentioned above and as shown in Table 5, EM 195 and Famenin contain solar-wind implanted noble gases, with e.g., $^{20}Ne/^{22}Ne$ ratios of 9.27 and 12.45, respectively. Note that the solar $^{20}Ne/^{22}Ne$ endmember of 12.45 measured for Famenin is in really good agreement with the range of values of e.g., 11.6 - 11.9 in Fayetteville (Wieler at al., 1989) or 12.4 in Frontier Mountain 90174 (Leya et al., 2009). This clearly indicates that EM 195 and Famenin were exposed as a regolith before their compaction and are regolith breccias.

Based on the quality assignments in Graf and Marti (1995), both meteorites have $^{20}Ne/^{22}Ne$ ratios which exceed the required conditions (i.e., $^{20}Ne/^{22}Ne > 2$; $^{36}Ar/^{38}Ar > 4.39$) defined by the authors. Based on their work, only meaningful cosmogenic concentrations and hence CRE ages can be calculated if the uncertainties due to the corrections of the trapped component are moderate. This is obviously not the case for both EM 195 and Famenin, with $^{20}Ne/^{22}Ne$ ratios of 9.27 and 12.45, respectively, and $^{36}Ar/^{38}Ar$ of 4.74 and 5.04, respectively (see Table 5). Consequently, the CRE ages for EM 195 and Famenin suffer from high uncertainties and should be considered with extreme caution. We will therefore refer in the following discussion as “nominal” CRE ages when evoking the CRE ages of EM 195 and Famenin.

Regarding lower T_{38} than T_{21} for EM 195 and Famenin, this trend has been already reported by Osawa and Nagao (2006). Several reasons can be invoked to explain this trend: first, by underestimating the ^{38}Ar production rates. As explained in Graf and Marti (1995), for shielding conditions where e.g., contributions of ^{36}Ar are due to radioactive

decay of neutron-capture produced ^{36}Cl, the amount of calculated trapped Ar can be overestimated therefore leading to wrong T_{38} ages. Given that the amount of neutron-capture nuclides increase with both size and shielding depth, calculation of CRE ages can be disturbed in the cases of large objects. Finally, one also has to bear in mind that the calculation of CRE ages for solar gas-rich meteorites is likely to be affected by erroneous shielding corrections. However, calculated T_{38} age seems quite consistent in the case of SJ 041. Additionally, one can invoke heterogeneities in the chemical composition within the samples, and in particular in the target elements for the production of ^{38}Ar (e.g., Ca), which could lead to some discrepancies. Note that we only measure samples between ~ 3 - 5 mg, which might introduce a bias considering the bulk composition of the meteorite, whereas the equations used for the production rates are for bulk compositions (e.g. Di Gregorio et al. 2019).

The nominal CRE ages for Famenin and EM 195 are generally older than the average values reported for H or L chondrites (Graf and Marti 1995; Marti and Graf 1992). The CRE age histogram for H chondrites in characterized by major peak centered around 6 - 10 Ma and another cluster identified around 33 Ma (Graf and Marti, 1995; Herzog and Caffee, 2014). Older CRE ages (i.e., T>40Ma) are observed to a lesser extent. Interestingly, the petrologic type H3 (to which Famenin belongs) has CRE age spanning from 5 - 40 Ma, without showing any cluster for CRE ages greater than 40 Ma (Herzog and Caffee, 2014). Our nominal CRE age data suggest that both Famenin and EM 195 were ejected at ~ 60 Ma, during an impact event different from those responsible for the ejection of the majority of H and L chondrites (Graf and Marti, 1995; Herzog and Caffee, 2014). However, as mentioned earlier in the discussion, these CRE ages are just nominal, and might suffer from high uncertainties due to huge corrections of the trapped component. A small cluster at ~ 60 Ma is observed (only 7 H chondrite members), except for H3 ordinary chondrites where such a peak is absent (Graf and Marti, 1995). Such old CRE ages would therefore suggests that EM 195 and Famenin may originate from a different parent body, or that both of the meteorites result in a slight deviation from the expected exponential distribution of ordinary chondrites associated with a continuous supply of meteoroids (Graf and Marti, 1995).

Chondrites intermediate between H and L groups

Mineralogical and oxygen isotope evidence indicate that ordinary chondrites originated from multiple parent bodies (Greenwood et al. 2020). In addition to the traditional H-L-LL sequence, accretion of ordinary chondrite parent bodies in conditions more reduced than for H chondrites, and intermediate between the three main groups (H/L and L/LL) have been described (Kallemeyn et al. 1989; Trigo-Rodríguez et al. 2009; Wittmann et al. 2011; Pourkhorsandi et al. 2017; Pratesi et al. 2019; Greenwood et al. 2020). This is in agreement with models indicating that the three main OC groups are portions of an incompletely sampled fractionation sequence (e.g., Müller et al., 1971). Based on this evidence, Greenwood et al. (2020) suggest between 3 to 6 parent bodies as the source of ordinary chondrites. Considering the gradual oxygen fugacity changes between different regions in the Solar nebula (e.g., Rubin 1990), the occurrence of meteorites originating from parent bodies with intermediate compositions between H and L chondrites is reasonable (Kallemeyn et al. 1989; Trigo-Rodríguez et al. 2009; Wittmann et al. 2011; Greenwood et al. 2020). Based on their fall date (between May and July), Trigo-Rodríguez et al. (2016) went further and suggested that Bremervörde, Tieschitz, Cali, and Famenin originated from a high-inclination stream of meteoroids formed as a result of disruption of comet C/1919 Q2 Metcalf. However, these meteorites do not have the expected properties of cometary materials (Campins and Swindle 1998; Greenwood et al. 2020).

In addition to Famenin, our work on Bremervörde, EM 195, and SJ 041 shows that these meteorites too have intermediate characteristics. One piece of evidence is the magnetic susceptibility values of Tieschitz, Bremervörde, Famenin, EM 195, and SJ 041 which are intermediate between mean H and L chondrite values (Rochette et al., 2001). It is also the case for some the samples with available saturation magnetization data (Gattacceca et al., 2014; Dekov et al., 2017). However, for SJ 041 because of its significant terrestrial weathering (W2 grade) this value cannot be interpreted as robustly in terms of original metal content, but it is more in agreement with L chondrite values (Rochette et al. 2012). SJ 041's Fa and Fs values are near the lower limits of L chondrites (Brearley and Jones 1998), but still are outside the limits recommended by

the Meteoritical Bulletin Nomenclature Committee for L chondrites (Grossman and Rubin, 2011). More importantly, its oxygen isotopic composition, especially $\Delta^{17}O$ is close to the field of Tieschitz, Bremervörde, and Famenin. For weathered meteorites, heavier composition (higher $\delta^{18}O$) can be explained by their high weathering degree which is shown to alter oxygen isotopic composition in this manner (Clayton and Mayeda 1991) or differences in the metamorphic history or conditions, or even pre-metamorphic alteration history (Reimold et al., 2004). As for SJ 041, the weathering products (oxides/oxyhydroxides) were removed before the isotopic analysis, the first scenario is less likely to be responsible for its relatively heavier composition. Such classification complications also is the case for EM 195 which with an intermediate log χ has average olivine and low-Ca pyroxene compositions of $Fa_{16.9\pm6.0}$ (n = 13) and $Fs_{17.2\pm5.6}Wo_{17.2\pm5.9}$ (n = 10), respectively that are in the range of H chondrites values (Brearley and Jones 1998). Meanwhile, similar to Famenin its average chondrule size is higher than in H chondrites. Oxygen isotopic composition of EM 195 is outside the range of equilibrated H and L chondrites. It should be noted that since the Bremervörde (H/L3.9), Tieschitz (H/L3.6), EM 195 (H/L3) and Famenin (H/L3.5/3.7) chondrites are unequilibrated their oxygen isotope composition is expected to show a larger scatter than for equilibrated ordinary chondrites, which prevents robust conclusions to be drawn from this dataset. The other interesting case is Gursum that caught our attention because of its intermediate log χ (5.09) (Rochette et al. 2003) and saturation magnetization (M_S = 28.9 Am^2kg^{-1}) (Gattacceca et al., 2014). Although based on mineral chemistry (Table 2), it is an H chondrite (close to the lower range), our oxygen isotope data put it away from the H chondrite field and within the L chondrite field (Fig. 7). However, it does not plot in the vicinity of H/L field but shows a similar $\Delta^{17}O$. Following these and the fact that Gursum is an equilibrated chondrite whose departing oxygen isotope composition cannot be related to heterogeneities found in unequilibrated chondrites, we suggest its classification to be updated to an H5-anomalous chondrite. Pavel is an anomalous H3 chondrite that has an intermediate log χ (5.11) and saturation magnetization (M_S = 26 Am^2kg^{-1}) in the range of L3 and L4 chondrites falls (Gattcceca et al., 2014), but its $\delta^{18}O$ is higher than H chondrites without a similarity to the intermediate chondrites studied here.

Table 8 lists 66 meteorites classified as intermediate chondrites in the Meteoritical Bulletin Database Database as of October 2021. The commonly used H/L designation is ambiguous. As described by Kallemeyn et al. (1989), H/L refers to the chondrites with bulk chemical properties intermediate between H and L chondrites. However, H/L is also often used by classifiers to describe meteorites whose assignation to H or L group is unclear, with a meaning close to the H(L) or L(H) classification. While some well-described meteorites such as Bremervörde, Cali, LaPaz Icefield (LAP) 031047 and Tieschitz are classified as H/L chondrites based on their truly intermediate characteristics (Kallemeyn et al. 1989; Trigo-Rodríguez et al. 2009; Wittmann et al. 2011), the majority of meteorites classified as H/L are simply H or L chondrites that have actually not been classified thoroughly for one or several reasons: unequilibrated mineral composition and low number of analyzed minerals, no estimate of chondrule size, lack of mineral chemistry data, and high weathering grade which decreases the efficiency of magnetic classification. Based on the characteristics of truly intermediate H/L chondrites (Bremervörde, Cali, EM 195, Famenin, LaPaz Icefield (LAP) 031047, SJ 041, and Tieschitz), we define ranges for their different characteristics as an attempt to identify the “real” intermediate H/L chondrites in the meteorite collection. We define the following criteria (Table 9): magnetic susceptibility (logχ) in the 4.95 - 5.20 range, for equilibrated ones (type 4 or higher) an average Fa content in the 20 - 24 mol% range, average apparent chondrule size in the L chondrites range (~ 500 µm), and $\Delta^{17}O$ between 0.8 and 1.2 ‰. After filtering out the poorly classified meteorites, we are left with a population of 36 H/L chondrites possibly truly distinct from H and L chondrites corresponding to 0.0006% of the total number of classified ordinary chondrites (56417), and that would deserve a specific classification nomenclature (Table 8). We propose to call these latter HL chondrites.

Olivine and low-Ca pyroxene data of HL chondrites show that except when they are unequilibrated chondrites (such as Famenin and EM 195), their olivine and low-Ca pyroxene composition is between H and L chondrite ranges (Fig. 9). This phenomenon is more evident in olivine Fa content (Fig. 13) as it equilibrates faster than low-Ca pyroxene during parent body thermal metamorphism (Dodd and Van Schmus, 1967). However, it becomes complicated in the case of some HL chondrites such as NWA series 4152-4156

(HL6) that have average Fa values of ~ 20, consistent with H chondrites, while average Fs value of ~ 20.4 and out of the range of H chondrites. Other characteristics for HL chondrites, such as oxygen isotopic composition, siderophile content, and metal abundance, suggest that they are indeed distinct chondrites. Considering the fact that meteorites are being classified mostly based on their olivine and low-Ca compositions, it is possible that some unequilibrated HL chondrites have been overlooked and classified either as H3 or L3 chondrites.

The existence of ordinary chondrites with properties outside of the usual ranges, such as the HL chondrites, can be accounted for by the existence of more than three parent bodies or by compositional heterogeneity of the three main parent bodies. This latter hypothesis would require extending the accepted ranges for the three main groups. Discriminating between the two hypotheses require a more detailed investigation using a larger and a multi-proxy database.

Hints for the existence of an HL chondrite cluster in the oxygen isotope dataset (Fig. 7) suggest that analyses of more equilibrated HL chondrites should be undertaken to validate the difference in oxygen isotopic composition between these chondrite and H-L-LL sequence. This also applies for noble gas composition measurements and CRE age distribution and comparison with those of the main ordinary chondrite groups. In addition, measurements of bulk rock and (Fe,Ni) metal compositions of the anomalous and intermediate ordinary chondrites would be helpful to unravel their relationship with the three main groups.

CONCLUSIONS

Famenin meteorite is a type 3.4/3.8 OC with characteristic distinct from the H and L chondrites. In addition to its primary characteristics (metal content, chondrule size, bulk composition, oxygen isotope composition, olivine and low-Ca pyroxene compositions etc.), Famenin's noble gas composition and CRE age distinguish it from the majority of H and L chondrites. Famenin along with 36 similar OCs might be member of another ordinary chondrite group originating from a different parent body than H, L, and LL chondrites, or originating from regions of these parent bodies that have rarely been

sampled. We propose to use a new designation (HL) for these meteorites rather than the ambiguous H/L designation that is also and mostly used for rather poorly characterized meteorites that could be either H or L chondrite. Following previous works on the diversity of ordinary chondrites, this work emphasizes again the existence of more than the three ordinary chondrite groups H, L, and LL, with possibly more than three associated parent bodies. Measuring oxygen isotopic composition of equilibrated HL chondrites, and CRE ages of a larger population of HL chondrites may help to test this hypothesis.

Acknowledgments

Behzad Qiasvand and *Nojum* magazine are thanked for their efforts in obtaining the Famenin meteorite samples for scientific studies. We thank I. Lefèvre (LSCE) for gamma spectroscopy. The first author thanks M. Zadsaleh for helping with the figures, and M. Djamali and D. Pourkhorsandi for their help during sample shipment. Cultural Office of the French Embassy in Tehran is acknowledged for providing Ph.D. grant for the first author. We thank the associate editor Dr. A. Ruzicka and reviewer Dr. J. Zipfel for a constructive review of the manuscript. V. Debaille and H. Pourkhorsandi thank the ERC StG “ISoSyC” and the FRS-FNRS. This project has received funding from the European Union’s Horizon 2020 research and innovation programme under the Marie Skłodowska-Curie grant agreement No 801505.

References:

Adib D., and Liou J. G. 1979. The Naragh meteorite - A new olivine-bronzite chondrite fall. *Meteoritics* 14:257–272.

Afiattalab F., and Wasson J. T. 1980. Composition of the metal phases in ordinary chondrites: implications regarding classification and metamorphism. *Geochimica et Cosmochimica Acta* 44:431–446.

Alexandre A., Basile-Doelsch I., Sonzogni C., Sylvestre F., Parron C., Meunier J.-D.,

and Colin F. 2006. Oxygen isotope analyses of fine silica grains using laser-extraction technique: Comparison with oxygen isotope data obtained from ion microprobe analyses and application to quartzite and silcrete cement investigation. *Geochimica et Cosmochimica Acta* 70:2827–2835.

Bonal L., Quirico E., Flandinet L., and Montagnac G. 2016. Thermal history of type 3 chondrites from the antarctic meteorite collection determined by Raman spectroscopy of their polyaromatic carbonaceous matter. *Geochimica et Cosmochimica Acta* 189:312–337.

Bouvier A., Gattacceca J., Agee C., Grossman J., and Metzler K. 2017. The Meteoritical Bulletin, No. 104. *Meteoritics & Planetary Science* 52:2284–2284.

Brearley A. J., and Jones R. H. 1998. Chondritic meteorites. *Reviews in Mineralogy and Geochemistry* 36 1–28

Campins H., and Swindle T. D. 1998. Expected characteristics of cometary meteorites. *Meteoritics & Planetary Science* 33:1201–1211.

Clarke R. S. 1975. The Meteoritical Bulletin. *Meteoritics* 10:133–158.

Clayton R., and Mayeda T. 1991. Oxygen isotope studies of ordinary chondrites. *Geochimica et Cosmochimica Acta* 55:2317–2337.

Consolmagno G. J., Macke R. J., Rochette P., Britt D. T., and Gattacceca J. 2006. Density, magnetic susceptibility, and the characterization of ordinary chondrite falls and showers. *Meteoritics & Planetary Science* 41:331–342.

Crespin J., Alexandre A., Sylvestre F., Sonzogni C., Paillès C., and Garreta V. 2008. IR Laser Extraction Technique Applied to Oxygen Isotope Analysis of Small Biogenic Silica Samples. *Analytical Chemistry* 80:2372-2378.

Dauphas N., and Pourmand A. 2015. Thulium anomalies and rare earth element patterns in meteorites and Earth: Nebular fractionation and the nugget effect. *Geochimica et Cosmochimica Acta* 163:234–261.

Decov V., Rochette P., Gattacceca J. 2017. Meteorite falls in Bulgaria: Reappraisal of

mineralogy, chemistry, and classification. *Meteoritics & Planetary Science* 52:1649–1659.

Di Gregorio M., Busemann H., Hunt A. C., Krietsch D., Schönbächler M., and Maden C. 2019. Variable cosmogenic argon in L/LL5 chondrite Knyahinya. In *82nd Annual Meeting of The Meteoritical Society*. p. 2157.

Dodd Jr. R. T., and Van Schmus W. R. 1967. A survey of the unequilibrated ordinary chondrites. *Geochimica et Cosmochimica Acta* 31:921–951.

Eugster O. 1988. Cosmic-ray production rates for 3He, 21Ne, 38Ar, 83Kr, and 126Xe in chondrites based on 81Kr-Kr exposure ages. *Geochimica et Cosmochimica Acta* 52:1649–1662.

Friedrich J. M., Wang M.-S., and Lipschutz M. E. 2003. Chemical studies of L chondrites. V: compositional patterns for 49 trace elements in 14 L4-6 and 7 LL4-6 falls. *Geochimica et Cosmochimica Acta* 67:2467–2479.

Garvie L. A. J. 2012. The Meteoritical Bulletin, No. 99, April 2012. *Meteoritics & Planetary Science* 47:E1–E52.

Gattacceca J., Suavet C., Rochette P., Weiss B. P., Winklhofer M., Uehara M., and Friedrich J. M. 2014. Metal phases in ordinary chondrites: Magnetic hysteresis properties and implications for thermal history. *Meteoritics & Planetary Science* 49:652–676.

Graf T., and Marti K. 1995. Collisional history of H chondrites. *Journal of Geophysical Research* 100:21247–21263.

Graham A. L. 1983. The Meteoritical Bulletin. *Meteoritics* 18:77–83.

Graham A. L., and Hassanzadeh J. 1990. The Meteoritical Bulletin. *Meteoritics* 25:59–63.

Greenwood R.C., Burbine T.H., Miller M.F., Franchi I.A. 2017. Melting and differentiation of early-formed asteroids: the perspective from high precision oxygen isotope studies. *Chemie der Erde* 77:1-43.

Greenwood R. C., Burbine T. H., and Franchi I. A. 2020. Linking asteroids and meteorites to the primordial planetesimal population. *Geochimica et Cosmochimica Acta* 277:377-406.

Grossman J. and Rubin A. (2011) White paper report for the Nomenclature Committee on the composition of olivine and pyroxene in equilibrated ordinary chondrites. 1-6. http://www.lpi.usra.edu/meteor/docs/whitepaper.pdf

Gröning M. 2004. Chapter 40 – International Stable Isotope Reference Materials. In *Handbook of Stable Isotope Analytical Techniques*. pp. 874–906.

Heber V. S., Wieler R., Baur H., Olinger C., Friedmann T. A., and Burnett D. S. 2009. Noble gas composition of the solar wind as collected by the Genesis mission. *Geochimica et Cosmochimica Acta* 73:7414–7432.

Herzog G. F. and Caffee M. W. 2014. Cosmic-ray exposure ages of meteorites. *Treatise on Geochemistry, 2nd Edition*. http://dx.doi.org/10.1016/B978-0-08-095975-7.00110-8.

Jarosewich E., Clarke, Clarke R. S., and Barrows J. N. 1987. Allende Meteorite Reference Sample. *Smithsonian Contributions to the Earth Sciences* 1–49.

Kallemeyn G. W., Rubin A. E., Wang D., and Wasson J. T. 1989. Ordinary chondrites: Bulk compositions, classification, lithophile-element fractionations and composition-petrographic type relationships. *Geochimica et Cosmochimica Acta* 53:2747–2767.

King A. J., Bates H. C., Krietsch D., Busemann H., Clay P. L., Schofield P.F., and Rusell S. S. 2019. The Yamato-type (CY) carbonaceous chondrite group: Analogues for the surface of asteroid Ryugu? *Meteoritics & Planetary Science* 79:1-17.

Leya I., Welten K. C., Nishiizumi K., and Caffee M. W. 2009. Cosmogenic nuclides in the solar gas-rich H3-6 chondrite breccia Frontier Mountain 90174. *Meteoritics & Planetary Science* 44:77-85.

Li S. J., Wang S. J., Miao B. K., Li Y., Li X. Y., Zeng X. J., and Xia Z. P. 2019. The density, porosity, and pore morphology of fall and find ordinary chondrites. *Journal of Geophysical Research: Planets* 124:2945-2969.

Marti K., and Graf T. 1992. Cosmic-Ray Exposure History of Ordinary Chondrites. *Annual Review of Earth and Planetary Sciences* 20:221–243.

Matsuda J., Matsumoto T., Sumino H., Nagao K., Yamamoto J., Miura Y., Kaneoka I., Takahata N., and Sano Y. 2002. The $^{3}He/^{4}He$ ratio of the new internal He Standard of Japan (HESJ). *Geochemical Journal* 36:191–195.

McCausland P.J.A., Flemming R.L., Mazur M.J., Umoh J., Holdsworth D.W., and Wengenroth J. 2016. Famenin, Iran ordinary chondrite 2015 fall: Non-destructive analysis. In *47th Lunar and Planetary Science Conference* pp. 3064–3065.

Megrue G. H., and Steinbrunn F. 1971. A search for “gas-rich” meteorites. In *Meteoritics*. pp. 292–293.

Metzler K. 2018. From 2D to 3D chondrule size data: Some empirical ground truth. *Meteoritics & Planetary Science* 53:1489-1499.

Metzler K.**,** Hezel D. C., Barosch J., Wölfer E., Schneider J. M., Hellmann J. L., Berndt J., Stracke A., Gattacceca J., Greenwood R., C.; Franchi I. A., Burkhardt C., and Kleine T. 2021. The Loongana (CL) group of carbonaceous chondrites. *Geochimica et Cosmochimica Acta* 304**:**1-31.

Miller M. F. 2002. Isotopic fractionation and the quantification of 17 O anomalies in the oxygen three-isotope system. *Geochimica et Cosmochimica Acta* 66:1881–1889.

Müller O., Baedecker P. A., and Wasson J. T. 1971. Relationship between siderophilic-element content and oxidation state of ordinary chondrites. *Geochimica et Cosmochimica Acta* 35:1121–1137.

Osawa T., and Nagao K. 2006. Noble gases in solar-gas-rich and solar-gas-free polymict breccias. *Antarctic Meteorite Research* 19:58–78.

Pourkhorsandi H., Gattacceca J., Devouard B., D’Orazio M., Rochette P., Beck P., Sonzogni C., and Valenzuela M. 2017. The ungrouped chondrite El Médano 301 and its comparison with other reduced ordinary chondrites. *Geochimica et Cosmochimica Acta* 218:98–113.

Ranjith P. M., He H., Miao B., Su F., Zhang C., Xia Z., Xie L., and Zhu R. 2017. Petrographic shock indicators and noble gas signatures in a H and an L chondrite from Antarctica. *Planetary and Space Science* 146:20–29.

Rao M. N., Garrison D. H., Bogard D. D., Badhwar G., and Murali A. V. 1991. Composition of solar flare noble gases preserved in meteorite parent body regolith. *Journal of Geophysical Research* 96:19321.

Reimold W. U., Buchanan P. C., Ambrose D., Koeberl C., Franchi I., Lalkhan C., Schultz L., Franke L., and Heusser G. 2004. Thuathe, a new H4/5 chondrite from Lesotho: History of the fall, petrography, and geochemistry. *Meteoritics & Planetary Science* 39:1321–1341.

Rochette P., Sagnotti L., Bourot-Denise M., Consolmagno G., Folco L., Gattacceca J., Osete M. L., and Pesonen L. 2003. Magnetic classification of stony meteorites: 1. Ordinary chondrites. *Meteoritics & Planetary Science* 38:251–268.

Rochette P. Gattacceca J., Lewandowski M. 2012. Magnetic classification of meteorites and application to the Soltmany fall. *Meteorites* 2:67-71.

Rubin A. E. 1990. Kamacite and olivine in ordinary chondrites: Intergroup and intragroup relationships. *Geochimica et Cosmochimica Acta* 54:1217–1232.

Ruzicka A., Grossman J., Bouvier A., Herd C. D. K., and Agee C. B. 2015. The Meteoritical Bulletin, No. 102. *Meteoritics & Planetary Science* 50:1662–1662.

Ruzicka A., and Hugo R. C. 2018. Electron backscatter diffraction (EBSD) study of seven heavily metamorphosed chondrites: Deformation systematics and variations in pre-shock temperature and post-shock annealing. *Geochimica et Cosmochimica Acta* 234:115–147.

Sears D. W., Grossman J. N., Melcher C. L., Ross L. M., and Mills A. A. 1980. Measuring metamorphic history of unequilibrated ordinary chondrites. *Nature* 287:791–795.

Schultz L., Weber H. W., and Begemann F. 1990. Planetary noble gases in H3- and H4-chondrite falls. *Meteoritics* 25:406–406.

Sears D. W., Grossman J. N., and Melcher C. L. 1982. Chemical and physical studies of type 3 chondrites—I: Metamorphism related studies of Antarctic and other type 3 ordinary chondrites. *Geochimica et Cosmochimica Acta* 46:2471–2481.

Stöffler D., Hamann C., and Metzler K. 2018. Shock metamorphism of planetary silicate rocks and sediments: Porposal for an update classification system. *Meteoritics & Planetary Science* 53:5–49.

Suavet C., Alexandre A., Franchi I. A., Gattacceca J., Sonzogni C., Greenwood R. C., Folco L., and Rochette P. 2010. *Identification of the parent bodies of micrometeorites with high-precision oxygen isotope ratios*. *Earth and Planetary Science Letters* 293:313-320.

Suess H. E., Wänke H., and Wlotzka F. 1964. On the origin of gas-rich meteorites. *Geochimica et Cosmochimica Acta* 28:595–607.

Takahito O., and Keisuke N. 2006. Noble gases in solar-gas-rich and solar-gas-free polymict breccias. *Antarctic Meteorite Research* 19:58–78.

Trigo-Rodríguez J. M., Llorca J., Rubin A. E., Grossman J. N., Sears D. W. G., Naranjo M., Bretzius S., Tapja M., and Sepúlveda M. H. G. 2009. The Cali meteorite fall: A new H/L ordinary chondrite. *Meteoritics & Planetary Science* 44:211–220.

Trigo-Rodríguez J. M., and Williams I. P. 2016. Are H/L chondrites associated with the disuptio of comet C/1919 Q2 Metcalf? *79th Annual Meeting of the Meteoritical Society* 6368.

Ward H. A. 1901. Veramin Meteorite. *American Journal of Science* s4-12:453–459.

Wasson J. T., and Kallemeyn G. W. 1988. Compositions of Chondrites. *Philosophical Transactions of the Royal Society A: Mathematical, Physical and Engineering Sciences* 325:535–544.

Weisberg M. K., McCoy T. J., and Krot A. N. 2006. Systematics and Evaluation of Meteorite Classification. *Meteorites and the Early Solar System II, D. S. Lauretta and H. Y. McSween Jr. (eds.), University of Arizona Press, Tucson, 943 pp.,* p. 19–52.

Weisberg M. K., Ebel D. S., Nakashima D., Kita N. T., and Humayun M. 2015. Petrology and geochemistry of chondrules and metal in NWA 5492 and GRO 95551: A new type of metal-rich chondrite. *Geochimica et Cosmochimica Acta* 167:269–285.

Wieler R., Baur H., Pedroni A., Signer P., and Pellas P. 1989. Exposure history of the regolithic chondrite Fayetteville: I. Solar-gas-rich matrix. *Geochimica et Cosmochimica Acta* 53:1441–1448.

Wittmann A. et al. 2011. H/L chondrite LaPaz Icefield 031047 – A feather of Icarus? *Geochimica et Cosmochimica Acta* 75:6140–6159.

Wlotzka F. 1993. A weathering scale for the ordinary chondrites. *Meteoritics* 28:460.

Figure captions:

Fig. 1: Picture showing a) the Famenin fall place on the roof of a house. Note a N-NW fall direction; b-d) Different fragments of the Famenin meteorite. (d) credit: A. Jamshidi.

Fig. 2: Optical micrographs of Famenin in transmitted polarized (a) and reflected (b) light.

Fig. 3: Optical (a & h) and BSE (b-g) images of Famenin. a) Note the fusion crust composed of magnetite, troilite veinlets, and vesicles. g) In this figure, a type I chondrule, smaller in size with Mg-rich olivine grains and metal droplets can be seen.

Fig. 4: Size frequency distribution of the chondrule diameters in Famenin, Pavel, and El Médano 195. Horizontal axis values mark the upper limits of the size bins.

Fig. 5: Composition of randomly chosen a) olivine (n = 71) and b) low-Ca pyroxene (n = 35) grains in Famenin.

Fig. 6: CI-normalized trace-element chemical composition of Famenin. Mean data for ordinary chondrites are from Wasson and Kallemeyn (1989).

Fig. 7: $\Delta^{17}O$ versus $\delta^{18}O$ values of our analyzed meteorites compared to type 3 (shown in white) and 4-7 (shown in black) H, L, and LL chondrites. Ochansk (H4), Paranaiba (L6), and Homestead (L5) were analyzed to check the accuracy of the measurement

and shown with numbers from 1 to 3, respectively. Ordinary chondrites with compositions intermediate between H and L are shown as HL (see text). The following chondrites that are anomalous and/or have intermediate compositions are shown with the following guide numbers: Pavel (4), Gursum (5), LAP 031047 (6), Bremervörde (7), EM 195 (8), Famenin (9), Bremervörde analyzed during our work (10), Tieschitz (11), and SJ 041 (12). Data sources: LAP 031047 (Wittmann et al. 2011), other samples (Clayton and Mayeda 1991) and the Meteoritical Bulletin Database (Table 2S). $\Delta^{17}O$ values are calculated as $\delta^{17}O - 0.52 \times \delta^{18}O$.

Fig. 8: Neon three-isotope diagram for EM 195 and Famenin. Also shown the Ne produced from Galactic Cosmic-Rays (GCR-Ne), Solar Cosmic-Rays (SCR-Ne), Air, and Solar Wind (SW). Errors bars are contained within the symbols and have been omitted for clarity. Dashed line indicates the mixing line between pure cosmogenic Ne and SW. Data from Heber et al. (2009).

Fig. 9: Average Fa vs. Fs (%mole) contents of olivine and low-Ca pyroxene of H, L, and LL chondrites, as well as the suggested HL chondrites (Table 8). Ordinary chondrites with compositions intermediate between H and L are shown as HL (more details in text). For H, L, and LL chondrites, only those with petrologic types ≥3.9 are shown. Type 3.9-4 H, L and LL chondrites are shown with empty circles while the type 5-7 chondrites are shown as filled circles. Standard deviation is indicated for type 3 HL chondrites. Data source for H, L, and LL chondrites: Meteoritical Bulletin Database (https://www.lpi.usra.edu/meteor/).

Fig. 10: a) Co content in kamacite vs. Fa%. Ordinary chondrites with compositions intermediate between H and L are shown as HL (more details in text). Chondrites and their corresponding numbers are: Djadjarm (1), Andila (2), Taqtaq-e Rasoul (3), Gursum (4), SJ 041 (5), EM 195 (6), Bremervörde (7), and Famenin (8). b) Co vs. Ni contents in kamacite of Famenin and ordinary chondrites. Chondrites and their corresponding numbers are: Djadjarm (1), Andila (2), Taqtaq-e Rasoul (3), Agen (4), Gursum (5), Tieschitz (6), EM 195 (7), Bremervörde (8), SJ 041 (9), and Famenin (10). Data source (including Bremervörde and Tieschitz): Rubin (1990). Pavel data from Dekov et al. (2017).

Fig. 11: Chemical composition of Famenin in comparison with ordinary chondrites. Ordinary chondrites with compositions intermediate between H and L are shown as HL (more details in text). Type 3-4 H, L and LL chondrites are shown with empty symbols while the type 5-7 chondrites are shown as filled symbols. Mean composition of H (red), L (blue), and LL (pink) together with individual chondrites are shown for comparison. Bulk rock data are from Wasson and Kallemeyn (1988) and Kallemeyn et al. (1989). Fayalite data are from Rubin (1990).

Fig. 12: Spectral parameters of Raman bands of carbonaceous materials in Famenin and in reference chondrites: $FWHM_D$ vs. I_D/I_G. Averages (points) and standard deviations (bars) are plotted for reference samples (black symbols) and for Famenin (open symbols). Spectral parameters of individual spectrum are plotted for Famenin (small grey diamonds). Reference chondrites data from Bonal et al. (2016).

Fig. 13: Relative frequency (%) distribution of Fa (mole%) contents for in H, L, LL, and HL (Table 8) chondrites. Ordinary chondrites with compositions intermediate between H and L are shown as HL (more details in text). Only ordinary chondrites with petrologic types ≥4 are included. Data source: (https://www.lpi.usra.edu/meteor/).

Electronic annex:

Fig. S1: Famenin fall location.

Fig. S2: Optical micrograph of El Médano 195 in reflected light.

Fig. S3: Optical microscopic image of San Juan 041 in reflected light.

Fig. S4: Optical microscopic image of Pavel in reflected light.

Fig. S5: Hysteresis properties of Famenin chondrite along with data for fall ordinary chondrites (from Gattacceca et al. 2014). Ordinary chondrites with compositions intermediate between H and L are shown as HL (more details in text).

Fig. S6: Bulk rock Ga versus fayalite composition of Famenin and ordinary chondrites. Ordinary chondrites with compositions intermediate between H and L are shown as HL (more details in text). Type 3-4 H, L and LL chondrites are shown with empty symbols

while the type 5-7 chondrites are shown as filled symbols. Mean composition of H (red), L (blue), and LL (pink) together with individual chondrites are shown for comparison. Bulk rock data are from Wasson and Kallemeyn (1988) and Kallemeyn et al. (1989). Fayalite data are from Rubin (1990).

Tables:

Table 1 (Pourkhorsandi et al.): Trace element (µg/g) determined by ICP-MS for Famenin and Allende as reference sample. Allende composition is reported from the literature for comparison.

Element	Famenin	Allende	Allende[a]	Allende[b]	Allende[c]
Li	1.57	1.58	-	1.5	-
Be	0.025	0.039	-	-	-
Ga	4.9	5.5	6 ± 1	6.15	-
Rb	3.01	1.17	1.2 ± 0.1	1.10	-
Sr	13.1	16.5	12 ± 3	-	-
Y	2.17	2.81	3.1 ± 0.1	3.10	-
Zr	5.8	7.1	9 ± 3	9.0	-
Nb	0.45	0.58	-	0.62	-
Cs	0.164	0.086	-	0.086	-
Ba	2.99	4.8	4 ± 1	4.00	-
La	0.30	0.51	0.52 ± 0.04	0.52	0.53
Ce	0.80	1.30	1.33 ± 0.08	1.33	1.38
Pr	0.12	0.20	0.21 ± 0.01	0.210	0.21
Nd	0.61	1.03	0.99 ± 0.03	0.99	1.07
Sm	0.20	0.32	0.34 ± 0.02	0.34	0.34
Eu	0.080	0.112	0.11 ± 0.01	0.11	0.12
Gd	0.27	0.40	0.42 ± 0.02	0.42	0.44
Tb	0.051	0.072	0.081 ± 0.010	0.081	0.08
Dy	0.34	0.48	0.42 ± 0.03	0.42	0.54
Ho	0.077	0.104	0.10 ± 0.01	0.10	0.11
Er	0.24	0.30	0.29 ± 0.01	0.29	0.31
Tm	0.034	0.054	-	0.0572	0.05
Yb	0.22	0.30	0.30 ± 0.02	0.30	0.33
Lu	0.034	0.046	0.052 ± 0.006	0.052	0.05
Hf	0.16	0.20	0.21 ± 0.01	0.21	-
Ta	0.024	0.040	-	-	-
W	0.11	0.17	-	0.167	-
Pb	0.22	1.27	1.39 ± 0.25		-

U	0.013	0.017	-	0.016	-
Sc	8.2	11.2	11 ± 1	11.0	-
Co	540	605	600 ± 100	612	-
Ni	13073	14800	14200 ± 200	-	-
Cu	74	104	119 ± 19	119	-
Zn	38	110	110 ± 5	117	-

The unit is µg/g. [a]Jarosewich et al. 1987. [b]Friedrich et al. 2003. [c]Dauphas and Pourmand 2015.

961 **Table 2 (Pourkhorsandi et al.):** Representative olivine and low-Ca compositions (in wt%) from Famenin, EM 195, and SJ
962 041.

	SiO_2	Al_2O_3	TiO_2	FeO	Cr_2O_3	MnO	MgO	CaO	Total	Fa (mol%)	Fs (mol%)
Famenin	41.90	0.04	0.03	6.11	0.65	0.43	49.99	0.09	99.25	6.39	-
	41.59	1.55	0.01	12.27	0.11	0.28	44.84	0.13	100.78	13.26	-
	40.79	0.03	0.00	14.40	0.14	0.27	45.45	0.10	101.18	15.05	-
	40.04	b.d.l.	b.d.l.	15.45	0.33	0.31	43.35	0.11	99.53	16.60	-
	39.81	0.03	0.03	15.63	0.17	0.30	43.70	0.13	99.79	16.65	-
	39.31	0.03	b.d.l.	16.69	0.06	0.28	42.91	0.07	99.35	17.85	-
	39.43	0.04	0.01	16.90	0.02	0.59	42.59	0.02	99.60	18.09	-
	39.86	b.d.l.	0.11	17.04	0.03	0.46	42.89	0.03	100.39	18.13	-
	39.95	0.01	0.02	17.06	0.00	0.38	42.78	0.02	100.22	18.20	-
	39.75	b.d.l.	0.01	17.09	0.02	0.45	42.36	0.03	99.71	18.37	-
	39.39	0.00	0.03	17.04	b.d.l.	0.50	42.16	0.01	99.12	18.38	-
	39.75	0.01	0.02	17.21	0.03	0.48	42.54	b.d.l.	100.03	18.40	-
	39.43	0.01	0.03	17.25	0.01	0.51	41.98	0.01	99.23	18.63	-
	39.52	0.02	0.02	17.37	0.00	0.43	42.28	0.04	99.68	18.64	-
	39.18	0.05	0.07	17.28	0.07	0.48	41.86	0.05	99.04	18.70	-
	40.13	0.05	0.02	17.20	0.37	0.42	41.55	0.05	99.79	18.75	-
	39.05	0.04	0.06	17.34	0.24	0.48	41.67	0.01	98.90	18.82	-
	39.36	b.d.l.	0.04	17.62	0.03	0.49	42.13	0.00	99.64	18.90	-
	40.17	0.25	0.04	17.38	0.15	0.47	41.20	0.08	99.74	19.03	-
	39.06	0.00	b.d.l.	18.11	0.00	0.45	41.76	0.01	99.37	19.47	-
	38.16	0.10	0.00	22.53	0.22	0.30	38.17	0.07	99.54	24.79	-
	58.67	0.36	0.07	3.63	1.11	0.58	34.16	1.97	100.56	-	6.27
	58.80	0.11	0.03	4.17	0.31	0.29	36.36	0.26	100.33	-	6.41
	56.77	0.14	0.13	10.88	0.12	0.52	30.99	0.68	100.21	-	16.90
	56.61	0.82	0.11	11.31	0.98	0.29	29.69	0.97	100.77	-	17.71
	55.11	0.05	0.01	17.62	0.59	0.66	25.44	0.29	99.78	-	28.67

	55.96	0.70	0.10	18.38	0.67	0.77	21.60	1.96	100.14	-	32.21
EM 195	38.62	n.d.	b.d.l.	20.62	n.d.	0.46	38.62	b.d.l.	98.31	23.05	-
	38.84	n.d.	b.d.l.	18.27	n.d.	0.39	40.41	b.d.l.	97.90	20.23	-
	39.02	n.d.	b.d.l.	17.02	n.d.	0.42	41.60	b.d.l.	98.06	18.67	-
	40.81	n.d.	b.d.l.	11.40	n.d.	0.03	46.60	b.d.l.	98.84	12.07	-
	40.07	n.d.	b.d.l.	17.48	n.d.	0.53	41.10	b.d.l.	99.18	19.27	-
	40.15	n.d.	b.d.l.	17.37	n.d.	0.45	40.87	b.d.l.	98.84	19.26	-
	40.39	n.d.	b.d.l.	15.40	n.d.	0.50	41.72	b.d.l.	98.01	17.16	-
	55.29	n.d.	0.23	11.26	n.d.	0.50	30.12	0.48	97.87	-	17.17
	56.65	n.d.	0.20	10.46	n.d.	0.50	30.55	0.39	98.75	-	15.99
	58.06	n.d.	b.d.l.	6.64	n.d.	0.34	33.35	0.16	98.54	-	10.02
	57.00	n.d.	0.19	10.91	n.d.	0.56	30.48	0.42	99.56	-	16.59
	53.83	n.d.	b.d.l.	18.47	n.d.	0.57	24.64	0.61	98.12	-	29.24
	57.89	n.d.	b.d.l.	5.69	n.d.	0.37	34.28	0.17	98.39	-	8.49
	55.42	n.d.	b.d.l.	14.75	n.d.	0.48	26.52	0.62	97.80	-	23.48
	57.28	n.d.	b.d.l.	10.63	n.d.	0.56	29.96	0.80	99.23	-	16.34
SJ 041	38.73	n.d.	n.d.	20.46	b.d.l.	0.47	39.97	0.00	99.62	22.31	-
	38.69	n.d.	n.d.	20.42	b.d.l.	0.51	40.00	0.00	99.62	22.27	-
	39.65	n.d.	n.d.	20.84	b.d.l.	0.43	40.16	0.00	101.08	22.55	-
	38.45	n.d.	n.d.	20.88	b.d.l.	0.49	39.81	0.00	99.63	22.74	-
	55.59	n.d.	n.d.	12.35	0.62	0.47	30.55	0.26	99.84	-	18.39
	55.57	n.d.	n.d.	12.03	0.37	0.46	30.57	0.63	99.62	-	17.88
	55.66	n.d.	n.d.	12.81	0.21	0.47	30.13	0.30	99.58	-	19.15
	56.53	n.d.	n.d.	11.48	0.36	0.45	30.88	0.34	100.04	-	17.15
	55.60	n.d.	n.d.	12.57	0.59	0.27	29.00	1.39	99.41	-	19.03
Gursum	37.36	n.d.	n.d.	14.61	0.03	0.54	44.50	0.00	97.12	15.55	-
	38.51	0.02	n.d.	15.19	n.d.	0.52	43.78	0.02	98.08	16.30	-
	38.62	0.01	0.02	14.86	0.02	0.53	44.35	0.00	98.46	15.83	-
	38.57	n.d.	n.d.	14.74	0.06	0.51	43.87	0.00	97.81	15.86	-
	38.05	0.01	0.02	15.33	n.d.	0.47	43.97	0.02	97.98	16.36	-

	55.19	0.19	0.26	9.67	0.21	0.60	31.46	0.76	98.38	-	14.50
	54.83	0.18	0.24	9.56	0.17	0.52	32.13	0.63	98.28	-	14.14
	53.86	0.17	0.22	9.73	0.15	0.66	32.14	0.74	97.76	-	14.31
	53.56	0.09	0.11	9.25	0.12	0.58	32.02	0.72	96.49	-	13.75
	55.35	0.18	0.12	9.59	0.08	0.61	32.04	0.68	98.65	-	14.20
	54.23	0.17	0.22	9.69	0.11	0.53	32.42	0.66	98.11	-	14.19

Detection limits (wt%) = Si (0.07), Al (0.06), Ti (0.13), Fe (0.16), Cr (0.07), Mn (0.14), Mg (0.07), Ca (0.05). b.d.l. = below detection limit. n. d. = not determined.

Table 3 (Pourkhorsandi et al.): (Fe,Ni) metal compositions (in wt%) in Famenin, EM 195, Gursum, and SJ 041.

Meteorite	Fe	Co	Ni	Total	Meteorite	Fe	Co	Ni	Total
Famenin	96.79	0.58	3.22	100.58	EM 195	93.71	0.30	6.65	100.66
	95.52	0.70	4.64	100.87		93.37	0.36	6.69	100.43
	94.99	0.75	5.21	100.95		93.32	0.20	6.67	100.48
	94.88	0.34	5.42	100.65		93.30	0.29	7.11	100.70
	94.48	0.34	6.64	101.4		92.65	0.28	6.72	99.65
	94.36	0.49	6.07	100.92		92.57	0.32	7.18	100.07
	93.86	0.56	6.70	101.11		92.36	0.34	7.09	99.78
	93.36	0.30	6.65	100.31		91.55	0.28	6.85	98.68
	93.16	0.48	6.40	100.04	Gursum	93.97	0.30	6.50	100.76
	93.16	0.25	6.89	100.29		93.24	0.15	6.41	99.80
	92.81	0.34	6.74	99.89		93.23	0.29	6.28	99.80
	92.63	0.30	6.85	99.78		93.00	0.23	6.31	99.53
	92.19	0.29	6.72	99.21		92.23	0.29	6.24	98.76
	91.90	0.59	6.11	98.60		91.84	0.41	6.73	98.98
	75.40	0.19	25.27	100.86		91.71	0.17	6.42	98.30
	72.80	0.22	27.81	100.82		91.68	0.21	6.26	98.15

	72.38	b.d.l.	27.97	100.36		72.96	b.d.l.	26.83	99.79
	68.52	b.d.l.	32.87	101.39		72.77	b.d.l.	27.42	100.19
	67.93	b.d.l.	32.47	100.40		72.28	b.d.l.	27.23	99.51
	67.83	b.d.l.	32.48	100.31	SJ 041	94.58	0.42	6.22	101.23
	67.73	b.d.l.	31.73	99.46		94.00	0.50	6.25	100.75
	66.99	b.d.l.	33.28	100.27		93.23	0.43	5.34	99.00
	66.13	b.d.l.	33.43	99.69		92.35	0.52	7.07	99.95
	65.98	b.d.l.	33.85	99.56		92.32	0.57	6.81	99.70
	65.01	b.d.l.	34.10	99.11		92.15	0.57	6.86	99.57
	64.00	b.d.l.	35.37	99.37		92.06	0.53	6.75	99.35
	52.52	b.d.l.	48.10	100.62		91.81	0.43	6.95	99.19
	48.69	b.d.l.	50.95	99.64		91.37	0.43	6.71	98.51
						58.47	b.d.l.	40.42	98.89

967 b.d.l. = below detection limit. Detection limits (wt%) = Fe (0.21), Co (0.18), Ni (0.18).

968

969 **Table 4 (Pourkhorsandi et al.):** Results of the whole rock oxygen isotopes analyses.

Meteorite	Group	$\delta^{18}O$ (‰)	$\delta^{17}O$ (‰)	$\Delta^{17}O$ (‰)	Bulk sample mass (mg)
Bremervörde	H/L3	5.53	3.84	0.96	27
El Médano 195	H/L3	5.01	3.41	0.81	
Famenin	H/L3	5.73	3.98	1.00	51
	H/L3	5.17	3.65	0.97	51
Gursum	H5-an	4.28	3.35	1.12	
Pavel	H3-an	5.05	3.26	0.63	27
Ochansk	H4	4.33	2.97	0.72	59
Homestead	L5	5.41	3.87	1.06	119
Paranaiba	L6	4.99	3.71	1.11	80
San Juan 041	H/L6	5.99	4.14	1.02	

970

Table 5 (Pourkhorsandi et al.): Measured He, Ne, and Ar concentrations and isotopic ratios in the studied meteorites.

Meteorite	Mass (mg)	^{3}He ($10^{-8}cm^3STP/g$)	$^{3}He/^{4}He$ ($\times10^{-4}$)	^{20}Ne ($10^{-8}cm^3STP/g$)	$^{20}Ne/^{22}Ne$	$^{21}Ne/^{22}Ne$	^{38}Ar ($10^{-8}cm^3STP/g$)	$^{36}Ar/^{38}Ar$	$^{40}Ar/^{36}Ar$
SJ 041	5.43	8.02±0.30	0.095±0.004	1.16±0.13	0.82±0.02	0.89±0.02	0.63±0.06	3.96±0.57	250±36
EM 195	3.06	0.28±0.03	6.65±0.13	60.2±6.9	9.27±0.02	0.19±0.01	2.62±0.27	4.74±0.69	535±78
Famenin	3.60	0.98±0.08	3.27±0.04	80.1±9.1	12.45±0.02	0.097±0.005	2.46 ±0.25	5.04±0.73	90±13

The given uncertainties (1σ) include the uncertainties for the ion current measurements and uncertainties caused by the corrections for interfering isotopes and corrections for instrumental mass fractionation. Systematic uncertainties in the calibration standard are included; they amount to about 4% for concentrations and 1% for isotope ratios.

Table 6 (Pourkhorsandi et al.): Cosmogenic He, Ne, and Ar concentrations and isotopic ratios in the studied meteorites.

Meteorite	Mass (mg)	$^{3}He_{cos}$* ($10^{-8}cm^3STP/g$)	$^{3}He/^{4}He$ ($\times10^{-4}$)	$^{21}Ne_{cos}$ ($10^{-8}cm^3STP/g$)	$(^{22}Ne/^{21}Ne)_{cos}$	$^{36}Ar_{cos}$ ($10^{-8}cm^3STP/g$)	$^{38}Ar_{cos}$
San Juan 041	5.43	8.02±0.30	0.095±0.004	1.76±0.20	1.12±0.06	0.232±0.026	0.368±0.042
El Médano195	3.06	0.28±0.03	6.65±0.13	1.13±0.13	1.95±0.10	0.116±0.013	0.184±0.021
Famenin	3.60	0.98±0.08	3.27±0.04	0.52±0.06	2.52±0.13	0.205±0.023	0.325±0.037

The given uncertainties (1σ) include the uncertainties for the ion current measurements and uncertainties caused by the corrections for interfering isotopes and corrections for instrumental mass fractionation. Systematic uncertainties in the calibration standard are included; they amount to about 4% for concentrations and 1% for isotope ratios.

*Assuming ^{3}He to be entirely cosmogenic.

Table 7 (Pourkhorsandi et al.): Production rates P_3, P_{21}, and P_{38} ($10^{-8}cm^3STP/g/Ma$) and cosmic-ray exposure ages T_3, T_{21}, and T_{38} (Ma).

Meteorite	Mass (mg)	P_3	T_3	P_{21}	T_{21}	P_{38}	T_{38}
SJ 041	5.43	1.61±0.06	4.99±0.60	0.332±0.004	5.30±0.6	0.042±0.005	8.71±0.99

EM 195	3.06	--	--	0.019±0.002	59.2±9.6	0.010±0.001	17.7±2.0
Famenin	3.60	--	--	0.0078±0.0009	66.4±7.6	0.0069±0.0008	47.4±5.4

Table 8 (Pourkhorsandi et al.): A list of meteorites classified with intermediate characteristics between H and L chondrites reported in the Meteoritical Bulletin and suggested HL chondrites.

Name	Class	Weathering grade	Fa (mol%)	Fs (mol%)	Magnetic Susceptibility	Saturation Magnetization (Am^2/kg)	Comments
Bremervörde*	H/L3.9	W0	18.6	-	4.97	15.12	-
Calama 085*	H(L)3	W3	20.3 ± 7.8	20.0±2.6	-	-	-
Cali*	H/L4	W0	22.8 ± 0.9	15.8 ± 6.9	5.11	-	-
Chug Chug 022*	L(H)3	W1	22.7 ± 8.28	14.5 ± 7.61	-	-	-
DaG[a] 369	L(H)3	W3	16.8 (9.3-27.4)	9.1 (4.4-17.7)	-	-	-
DaG 378	H(L)3	W2	14.3 (0.9-26.6)	7.9 (2.1-25.2)	-	-	-
DaG 591	H(L)6	W3	20	17.4	-	-	Highly weathered
Dhofar 428*	H/L5	W4	21.5	18.5	-	-	-
Dhofar 1022	H(L)3-an	W4	18.5 ± 1.3	16.5 ± 5.5	-	-	
Dhofar 1035	H(L)3	W4	21 ± 4	15.5 ± 3.5	-	-	Highly weathered
Dhofar 2058	H(L)6	W4	-	-	4.67	-	Needs average Fa data
EM[b] 195*	H/L3	W1	16.9 ± 6.0	17.2 ± 5.6	4.99	-	-
Famenin*	H/L3	W0	17.4 ± 3.7	17.1 ± 9.0	5.09	24.9	-
Gursum	H5-an	W0	16.0 ± 0.3	14.2 ± 0.2	5.09	28.88	-
Haxtun*	H/L4	W4	21.6 ± 0.4	17.8 ± 1.3	-	-	-
JaH[c] 113	H/L4	W2	-	-	4.9	-	Needs average Fa data

JaH 805	L(H)3	W3	12.6 – 34.2	7.7 – 15.7	4.8	-	Highly weathered
Königsbrück*	H/L4	W1	22.6	8.2 – 20.1	-	-	-
LAP[d] 031047*	H/L	A	23	17	-	-	Needs more work
NWA[e] 1518*	H/L3	W2	21	18.3	-	-	-
NWA 1534*	H/L4	W2	20.5	17.6	-	-	-
NWA 1554	L/H4	W3	-	-	5	-	Needs average Fa data
NWA 1955	H/L3-4	-	20.6	20.44	-	-	-
NWA 1976	L(H)3	W3	14.5 ± 8	11 ± 8	-	-	-
NWA 2001*	H/L4	W0	22	19.3	5.21	-	-
NWA 2521	H/L3	W2	18.2 ± 7.3	14.3 ± 6.1		-	Needs average Fa data
NWA 2617	H/L4	W2	19.5 - 20.5	16.2 - 21.2	4.93	-	Needs average Fa data
NWA 3330*	H/L5	W3	21.8	18.8	-	-	-
NWA 3342	H/L4	W1	17 - 28	11.2 - 19.9	-	-	Needs average Fa data
NWA 4089*	H/L4/5	W3	21.2	18.1	-	-	-
NWA 4097	H/L3	W2	7.9 - 24	4.7 - 18.8	-	-	Needs average Fa data
NWA 4150	H/L6 Imc	W0/1	24.1	19.9	-	-	-
NWA 4152*	H/L6	W2	20.4	20.4	-	-	-
NWA 4153*	H/L6	W3	20.1	20.1	-	-	-
NWA 4154*	H/L6	W4	20.6	20.6	-	-	-
NWA 4155*	H/L6	W3	21.2	21.2	-	-	-
NWA 4156*	H/L6	W3	19.9	19.9	-	-	-

NWA 4334	H/L3	W1	2.0 - 30.0	4.3 - 17.2	-	-	Needs average Fa data
NWA 4357	H/L3	W1	3.7 - 31.1	2 - 24.3	-	-	Needs average Fa data
NWA 4725	H/L3	W2	16.3 ± 9.1	5.17 ± 3.09	-	-	Needs average Fa data
NWA 4726	L/H5	W2	24.67 ± 0.31	22.06 ± 1.33	4.98	-	Needs average Fa data
NWA 5809*	H/L5	W3	20.7	17.5 - 18.2	4.95	-	-
NWA 5945*	H/L3	-	24.2 ± 2.0	14.5 ± 5.7	-	-	-
NWA 7327*	H/L5	W3	20.5 ± 0.3	18.4 ± 1.5	-	-	-
NWA 8123	H(L)3.1	W2/3	0.3 – 97.1	2.0 – 12.7	4.02	-	Needs average Fa data, low logx
NWA 8793	H(L)3	W2/3	11.3 – 30.6	4.5 – 15.2	4.68	-	Needs average Fa data
NWA 10287*	H/L5	W0/1	21.7 - 21.9	18.4 - 19.1	5.2	-	-
NWA 11570*	H/L4	W5	21.7 ± 1.0	17.6 ± 6.6	-	-	-
NWA 13520	L(H)3	W2	16.9 ± 6.4	9.4 ± 5.4	-	-	Needs magnetic data
Pavel	H3-an	W0	19.7 ± 1.9	19.0 ± 6.3	5.11	26	-
SJ[f] 041*	H/L6	W2	22.5 ± 0.2	18.3 ± 0.8	4.59	-	-
SaU[g] 147	H/L4	W3	19.5	17.2	-	-	-
SaU 185	L/H4-5	W2	19.4 - 24.5	17.2 - 20.6	-	-	-
SaU 301	H/L4	W1	19.0 - 20.0	16.6 - 19.2	4.99	-	-
SaU 324	H/L6	W3/4	20.3	17.6	-	-	-
Sierra Gorda 028*	H/L5	W1	21.8 ± 0.24	18.4 ± 0.32	-	-	-
Tieschitz*	H/L3.6	W0	-	-	4.98	16.79	
Y[h]-74645*	H/L4	-	21.1	17.9	-	-	

Y-9405	H/L4	-	-	-	-	-	Needs more data
Y-983336*	H/L5	B	21	19.2	-	-	-
Y-983388*	H/L6	C	21.1	18.3	-	-	-
Y-983430*	H/L5	A/B	20.9	18.4	-	-	-
Y-983551*	H/L6	C	21.5	18.5	-	-	-
Y-983629*	H/L6	A/B	20.9	18.5	-	-	-
Y-983931*	H/L4	A/B	21.3	13.2	-	-	-
Y-000746	H/L4-5	B/C	20.3	14.6	-	-	-
Y-000782*	H/L4	B/C	21	18.5	-	-	-

[a]Dar al Gani, [b]El Médano, [c]Jiddat al Harasis, [d]LaPaz Icefield, [e] Northwest Africa, [f]San Juan, [g]Sayh al Uhaymir, [h] Yamato.

Data source: Meteoritical Bulletin. Mineral chemistry, magnetic susceptibility, and saturation magnetization data for Bremervörde are from Rubin (1990), Rochette et al. (2003), and Gattacceca et al. (2014), respectively. Same data for Cali and Pavel are from Trigo-Rodríguez et al. (2009) and Dekov et al. (2017), respectively. Magnetic susceptibility and saturation magnetization data of Tieschitz and Gursum from Rochette et al. (2003) and Gattacceca et al. (2014), respectively.

Table 9 (Pourkhorsandi et al.): Suggested criteria for classifying HL chondrites.

Criteria	Suggested values
Magnetic susceptibility (log χ)	4.95-5.20
Average chondrule size (μm)	~ 500
Fa content (mol%)	20-24
$\Delta^{17}O$ (‰)	0.8-1.2

Table 1S (Pourkhorsandi et al.): (Fe,Ni) metal compositions (in wt%) of Catalina 396, Taqtaq-e Rasoul, Agen, Andila, Djadjarm, Ausson, and Bensour.

Meteorite	Fe (wt%)	Ni (wt%)	Co (wt%)	Total
Catalina 396 (H6)	94.44	6.86	0.43	101.73
Catalina 396 (H6)	95.16	7.09	0.52	102.76
Taqtaq-e Rasoul (H5)	66.65	34.97	b.d.l.	101.52
Taqtaq-e Rasoul (H5)	67.68	32.84	0.15	100.67
Taqtaq-e Rasoul (H5)	68.03	32.30	0.14	100.55
Taqtaq-e Rasoul (H5)	93.85	6.46	0.35	100.76
Taqtaq-e Rasoul (H5)	93.92	6.68	0.42	100.99
Taqtaq-e Rasoul (H5)	94.09	6.42	0.35	100.85
Taqtaq-e Rasoul (H5)	94.34	6.48	0.31	101.16
Taqtaq-e Rasoul (H5)	94.75	6.38	0.59	101.71
Taqtaq-e Rasoul (H5)	94.79	5.76	0.16	100.73
Agen (H5)	50.11	48.43	b.d.l.	98.53
Agen (H5)	92.01	5.97	0.38	98.83
Agen (H5)	93.28	6.29	0.40	100.01
Agen (H5)	93.35	6.09	0.27	99.79
Agen (H5)	93.50	6.19	0.37	100.01
Agen (H5)	93.58	5.71	0.51	99.82
Agen (H5)	93.92	5.71	0.47	100.09
Andila (L6)	44.56	54.19	0.19	98.97
Andila (L6)	60.32	38.40	0.12	98.93
Andila (L6)	72.70	26.61	0.23	99.49
Andila (L6)	74.54	25.58	0.49	100.65

Andila (L6)	92.99	6.17	0.73	99.86
Andila (L6)	93.60	5.98	0.77	100.40
Andila (L6)	93.93	4.82	0.96	99.79
Andila (L6)	93.95	6.47	0.80	101.25
Andila (L6)	94.04	6.61	0.45	101.07
Djadjarm (L6)	46.13	51.74	0.03	97.91
Djadjarm (L6)	58.03	32.06	0.03	90.17
Djadjarm (L6)	61.28	37.08	0.03	98.47
Djadjarm (L6)	94.39	6.72	0.96	102.19
Djadjarm (L6)	94.49	6.32	0.70	101.55
Djadjarm (L6)	95.18	6.10	0.86	102.10
Ausson (L5)	58.92	37.54	0.04	96.54
Ausson (L5)	59.63	38.35	b.d.l.	97.93
Ausson (L5)	65.85	32.33	0.03	98.29
Ausson (L5)	66.47	31.32	0.08	97.89
Ausson (L5)	77.99	18.59	0.73	97.42
Ausson (L5)	78.67	18.55	0.56	97.81
Bensour (LL6)	51.09	45.94	1.74	98.85
Bensour (LL6)	51.59	45.98	1.81	99.29
Bensour (LL6)	62.86	0.03	b.d.l.	97.83
Bensour (LL6)	63.05	b.d.l.	b.d.l.	98.18
Bensour (LL6)	63.38	0.00	0.06	98.57
Bensour (LL6)	63.55	b.d.l.	b.d.l.	98.70

b.d.l. = below detection limit. Detection limits (wt%) = Fe (0.21), Co (0.18), Ni (0.18).

1002 **Table 2S (Pourkhorsandi et al.):** Whole-rock oxygen isotopes composition of ordinary chondrites.

Meteorite	Class	$\delta^{18}O$	$\delta^{17}O$	$\Delta^{17}O$
Dhajala	H3	4.12	2.84	0.70
Sharps	H3	3.95	2.70	0.65
RaSa 430	H3	5.12	3.17	0.51
JaH 567	H3	5.55	3.63	0.74
NWA 1709	H3	4.45	2.84	0.53
NWA 3358	H3	4.67	2.91	0.48
NWA 8061	H3	5.78	3.32	0.32
Bath	H4	4.19	2.89	0.71
Beaver Creek	H4	4.27	2.98	0.76
Kesen	H4	4.51	2.98	0.63
Ochansk	H4	3.85	2.82	0.82
Tysnes Island	H4	4.19	2.88	0.70
Weston	H4	4.08	3.00	0.88
Thuathe	H4/5	4.55	3.12	0.75
Carancas	H4/5	4.43	2.98	0.68
Allegan	H5	3.97	2.68	0.61
Ambapur Nagla	H5	3.94	2.80	0.75
Beardsley	H5	4.20	2.93	0.75
Forest Vale	H5	3.82	2.64	0.65
Glenrothes	H5	4.21	2.69	0.50
Leighton	H5	3.87	2.88	0.87
Mason Gully	H5	4.42	3.04	0.74
Pantar	H5	4.09	2.69	0.56
Richardton	H5	4.08	2.74	0.61
Tamdakht	H5	5.01	3.26	0.65
Cape Girardeau	H6	3.79	2.69	0.72
Charsonville	H6	3.83	2.64	0.65
Dhofar 1559	H6	4.62	3.00	0.59
Guareña	H6	4.10	2.89	0.76
Kernouve	H6	4.15	2.94	0.78
Mount Browne	H6	3.88	2.71	0.69

Križevci	H6	3.99	2.76	0.68
Towada	H6	4.04	2.79	0.69
Queen's Mercy	H6	4.08	2.84	0.72
Xingyang	H6	3.89	2.83	0.81
NWA 2898	H7	4.4	2.90	0.62
NWA 4226	H7	4.64	3.18	0.77
NWA 4229	H7	4.40	3.03	0.74
NWA 7024	H7	4.24	2.83	0.63
NWA 8400	H7	4.64	2.93	0.52
NWA 12236	H7	4.50	2.94	0.60
Bremervörde	H/L3	4.57	3.35	0.97
Tieschitz	H/L3	5.55	3.83	0.94
Aba Panu	L3	5.08	3.68	1.04
Catalina 001	L3	5.15	3.66	0.98
Dhofar 2056	L3	4.74	4.03	1.57
Hallingeberg	L3	4.79	3.33	0.84
Khohar	L3	4.52	3.48	1.13
Mezö-Madaras	L3	4.81	3.45	0.95
NWA 6744	L3	5.05	3.43	0.80
NWA 6745	L3	5.26	3.54	0.80
NWA 6864	L3	5.87	3.84	0.79
NWA 6925	L3	5.57	4.04	1.14
NWA 8257	L3	4.64	3.27	0.86
NWA 8258	L3	5.38	3.66	0.86
NWA 8276	L3	4.79	3.05	0.57
NWA 10774	L3	5.39	3.84	1.04
RdDL 067	L3	5.48	3.77	0.92
SaU 564	L3	4.83	3.63	1.12
Hedjaz	L3-6	4.57	3.51	1.13
Atarra	L4	4.88	3.68	1.14

Bjurböle	L4	4.90	3.55	1.00
Clarendon (c)	L4	4.88	3.66	1.13
Cynthiana	L4	5.44	3.91	1.08
Kendleton	L4	4.61	3.43	1.03
Saratov	L4	4.74	3.48	1.02
Tennassilm	L4	4.56	3.52	1.15
NWA 10954	L4	4.05	3.11	1.01
NWA 7556	L4-6	5.36	3.87	1.08
Ausson	L5	4.60	3.53	1.14
Barwell	L5	4.63	3.57	1.17
Borkut	L5	4.61	3.46	1.06
Chervettaz	L5	4.64	3.66	1.25
Elenovka	L5	4.56	3.44	1.07
Ergheo	L5	5.00	3.58	0.98
Farmington	L5	4.80	3.63	1.13
Homestead	L5	4.62	3.52	1.12
Knyahinya	L5	4.99	3.64	1.05
Mifflin	L5	4.84	3.65	1.13
NWA 11744	L5	5.14	3.78	1.11
NWA 11745	L5	4.93	3.69	1.13
NWA 12386	L5	4.81	3.55	1.05
NWA 13192	L5	5.23	3.88	1.16
NWA 13193	L5	4.78	3.64	1.16
Park Forest	L5	4.69	3.44	1.00
Qidong	L5	4.95	3.66	1.09
Mocs	L5-6	4.55	3.50	1.13
Renchen	L5-6	4.74	3.63	1.17
Bachmut	L6	4.40	3.45	1.16
Bori	L6	4.62	3.46	1.06
Cabezo de Mayo	L6	5.02	3.65	1.04
Katol	L6	4.91	3.57	1.02
Leighlinbridge	L6	4.44	3.46	1.15
Modoc (1905)	L6	4.65	3.50	1.08

Nan Yang Po	L6	4.40	3.26	0.97
NWA 8684	L6	5.15	3.88	1.20
NWA 13194	L6	4.98	3.67	1.08
NWA 13195	L6	4.85	3.61	1.09
NWA 13196	L6	5.20	3.83	1.12
Tathlith	L6	4.33	3.40	1.15
Tillaberi	L6	4.54	3.33	0.97
Viñales	L6	4.54	3.48	1.12
Xiujimgin	L6	4.51	3.41	1.06
Dhofar 008	L7	5.67	3.81	0.86
PAT 91501	L7	4.7	3.7	1.26
Bishunpur	LL3	6.00	4.11	0.99
Chainpur	LL3	5.72	4.01	1.04
Krymka	LL3	5.60	4.09	1.18
Manych	LL3	5.37	3.75	0.96
Ngawi	LL3	5.40	3.98	1.17
NWA 2748	LL3	7.21	4.89	1.14
NWA 3260	LL3	5.65	3.57	0.63
NWA 4522	LL3	5.55	3.84	0.95
NWA 6082	LL3	5.95	3.83	0.74
NWA 6742	LL3	6.36	4.24	0.93
NWA 6867	LL3	5.66	3.54	0.60
NWA 8059	LL3	4.40	2.55	0.26
NWA 8124	LL3	5.16	3.00	0.32
NWA 8649	LL3	5.01	3.25	0.65
NWA 10786	LL3	5.28	3.66	0.91
Parnallee	LL3	5.15	3.82	1.14
SaU 565	LL3	4.95	3.72	1.15
Semarkona	LL3	6.09	4.24	1.07
St. Mary's County	LL3	5.66	4.18	1.24
Vicência	LL3	5.36	3.77	0.98
Albareto	LL4	5.31	3.96	1.20
Bo Xian	LL4	5.58	4.06	1.16

Hamlet	LL4	5.31	4.12	1.36
Savtschenskoje	LL4	5.10	3.94	1.28
Soko Banja	LL4	4.85	3.85	1.33
Witsand Farm	LL4	5.32	4.12	1.35
Guidder	LL4-6	4.77	3.67	1.19
NWA 8691	LL4-6	5.67	3.98	1.03
Khanpur	LL5	5.03	4.03	1.41
Olivenza	LL5	4.88	3.66	1.13
Paragould	LL5	5.11	4.05	1.39
Siena	LL5	5.32	4.09	1.32
Appley Bridge	LL6	5.07	3.93	1.29
Bensour	LL6	5.30	4.00	1.24
Dhurmsala	LL6	5.09	3.80	1.15
Dongtai	LL6	5.08	3.66	1.02
Ensisheim	LL6	4.80	3.90	1.40
Jelica	LL6	4.76	3.75	1.27
Mangwendi	LL6	4.75	3.91	1.44
NWA 6503	LL6	5.30	3.98	1.23
NWA 7988	LL6	5.03	3.82	1.20
NWA 12575	LL6	5.48	4.03	1.18
St. Mesmin	LL6	5.13	3.80	1.13
Saint-Séverin	LL6	4.76	3.63	1.15
Vavilovka	LL6	4.83	3.72	1.21
NWA 969	LL6/7	5.30	4.00	1.24
JaH 513	LL7	5.73	4.07	1.09
NWA 6426	LL7	4.75	3.71	1.24
NWA 7030	LL7	6.15	4.36	1.16
NWA 10103	LL7	5.19	3.93	1.24
NWA 12534	LL7	5.36	4.02	1.23
NWA 12921	LL7	5.59	4.26	1.35

1003 Data source: Clayton & Mayeda (1991) and Meteoritical Bulletin Database (https://www.lpi.usra.edu/meteor/).


a
Running Head
South

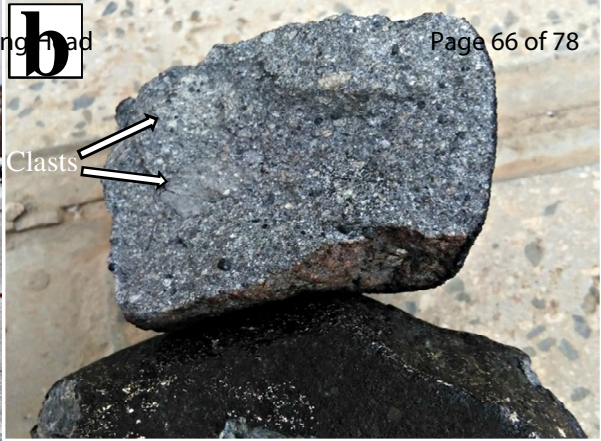
b
Clasts


c

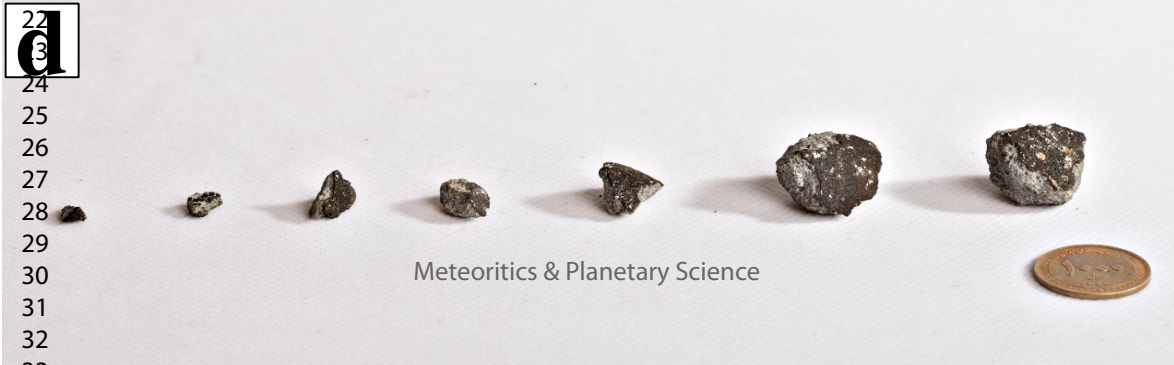
d

a

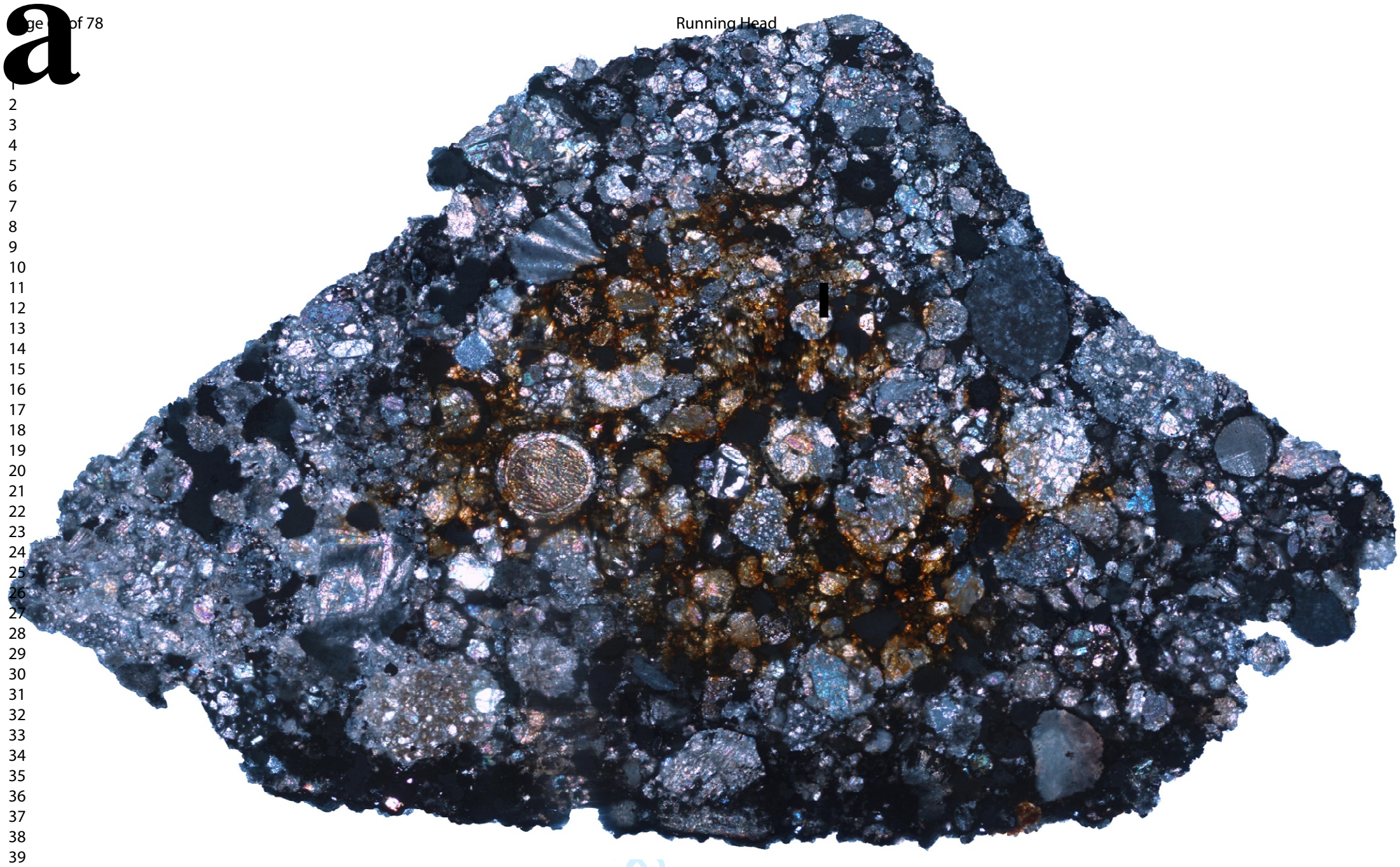

Famenin

3.5 mm

b

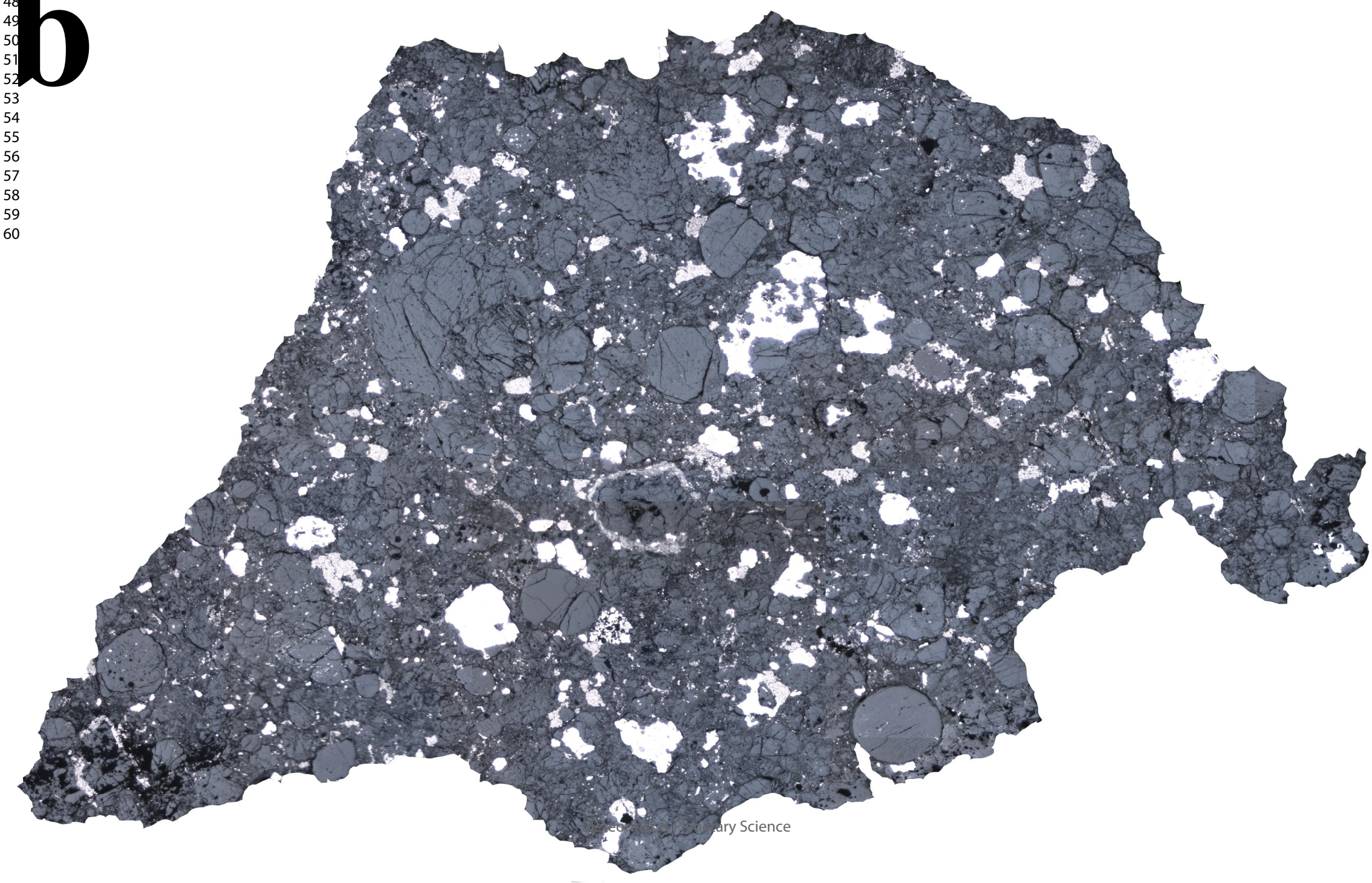

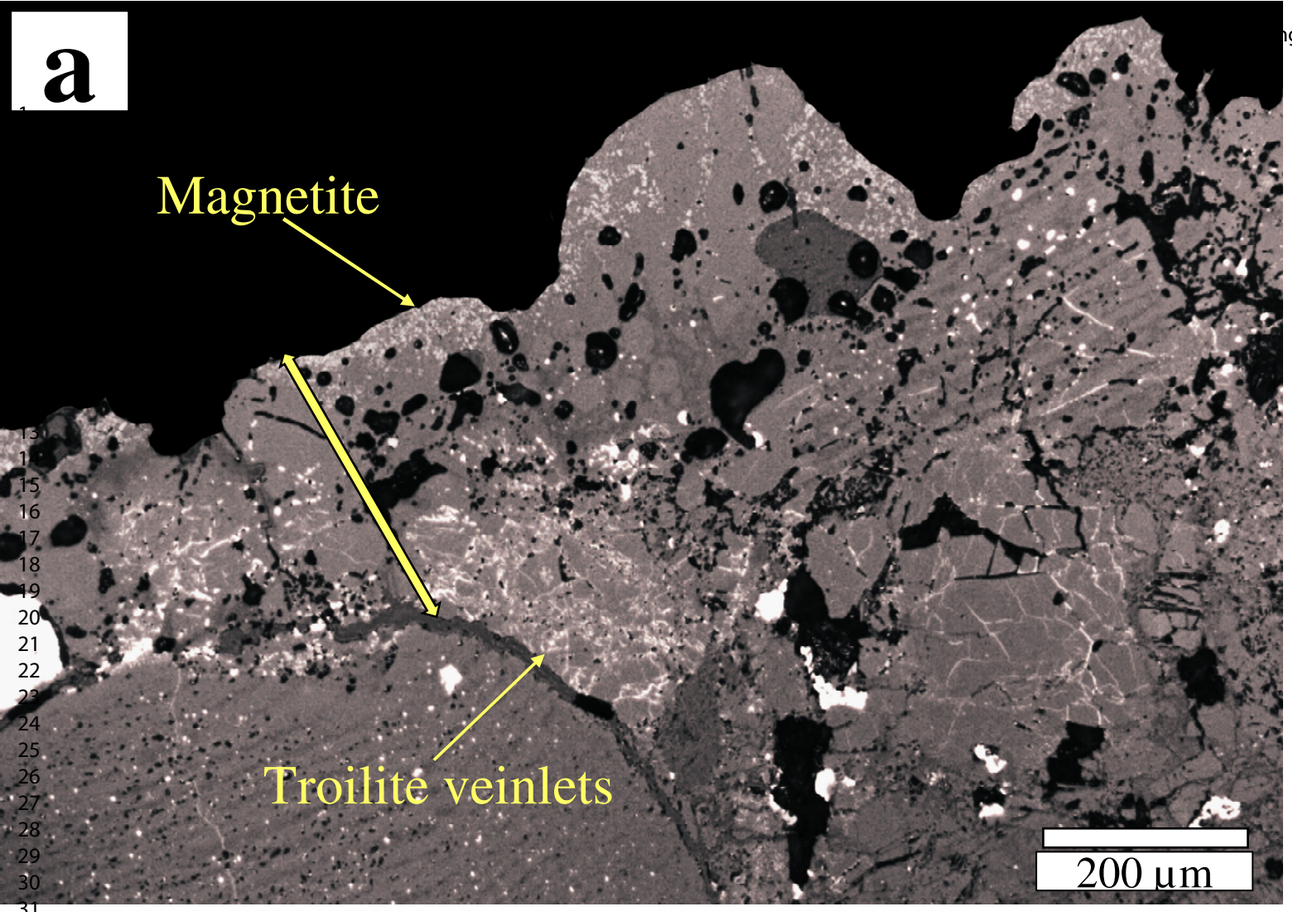
a
Magnetite
Troilite veinlets
200 µm

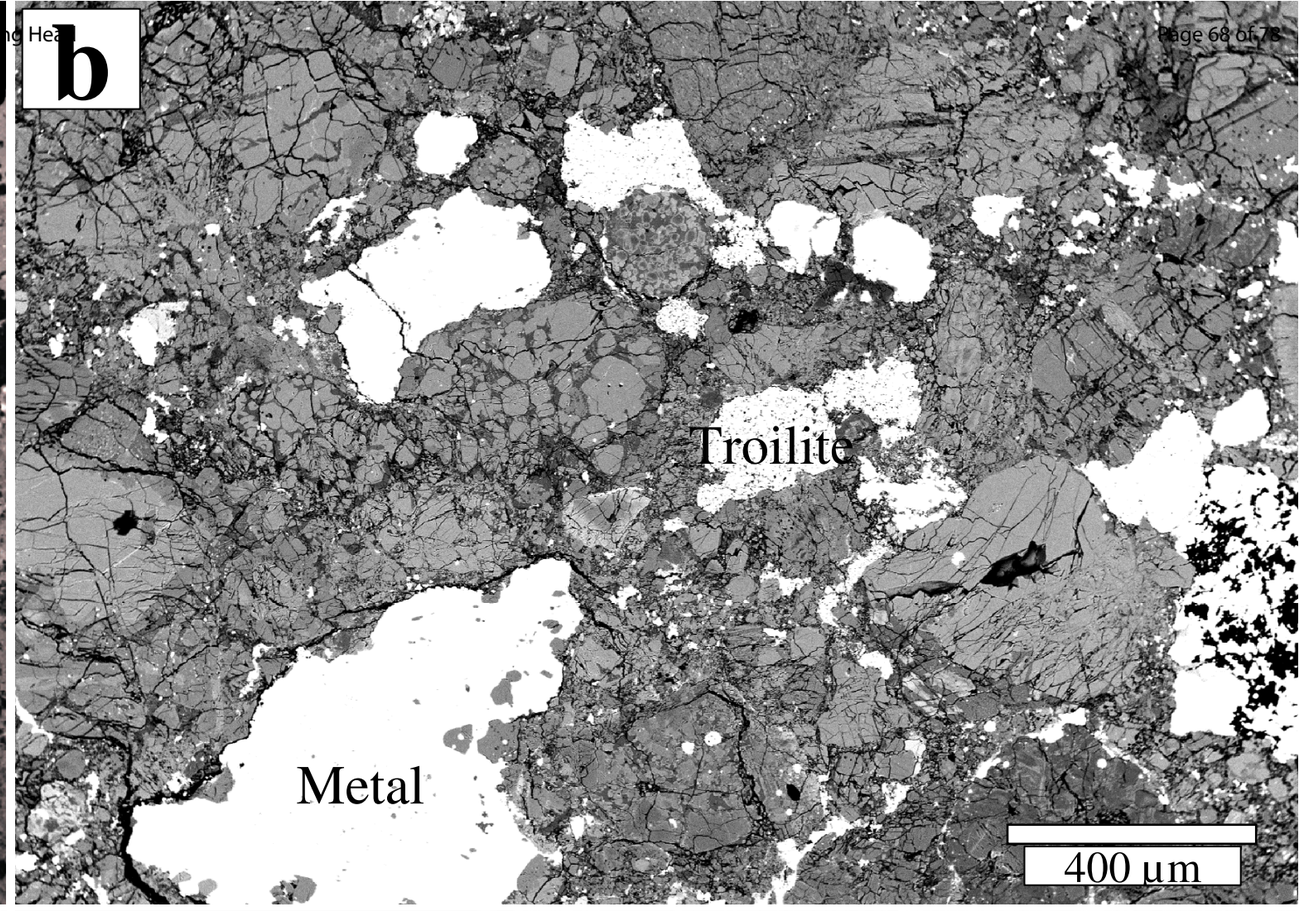
b
Troilite
Metal
400 µm

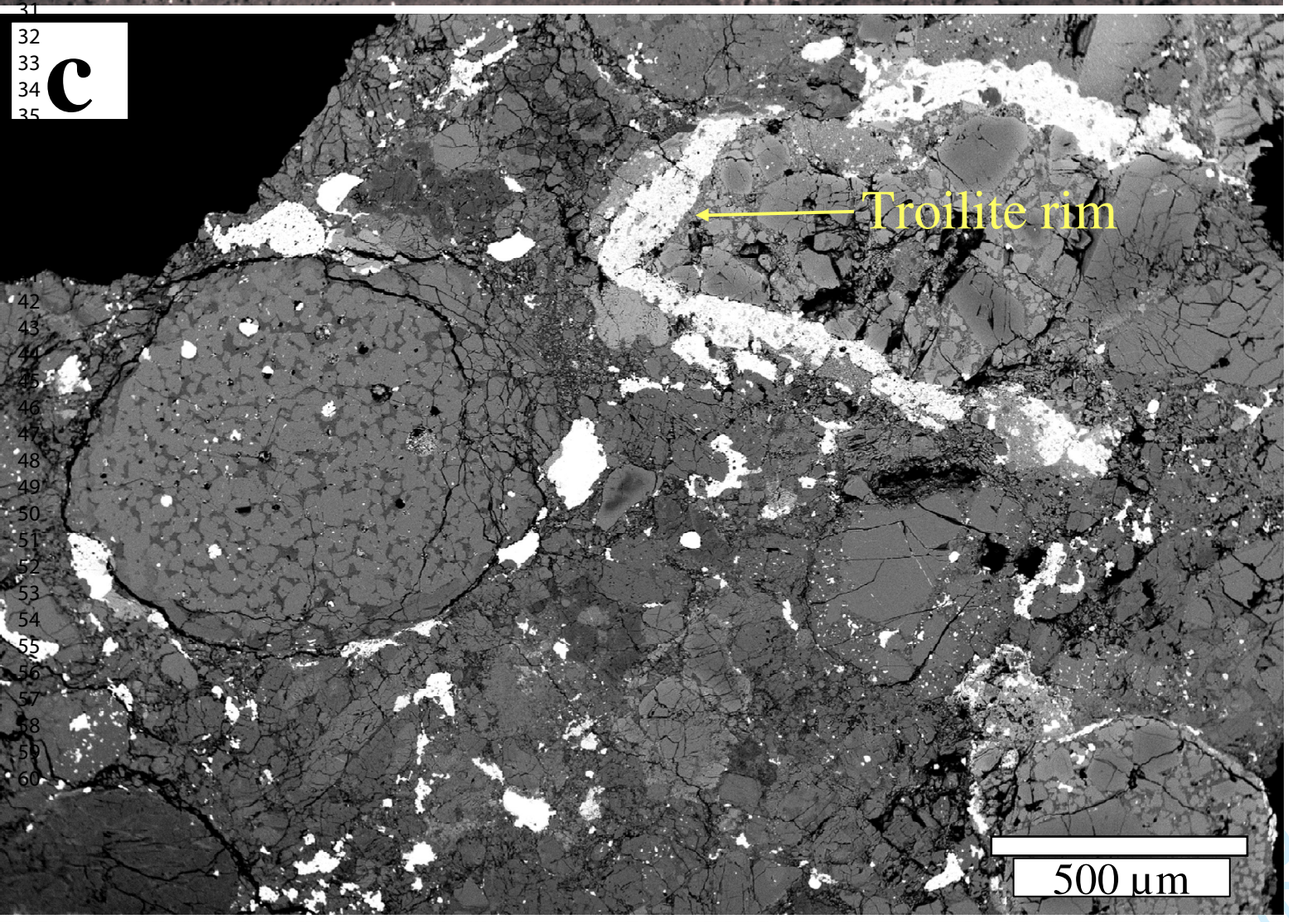
c
Troilite rim
500 µm

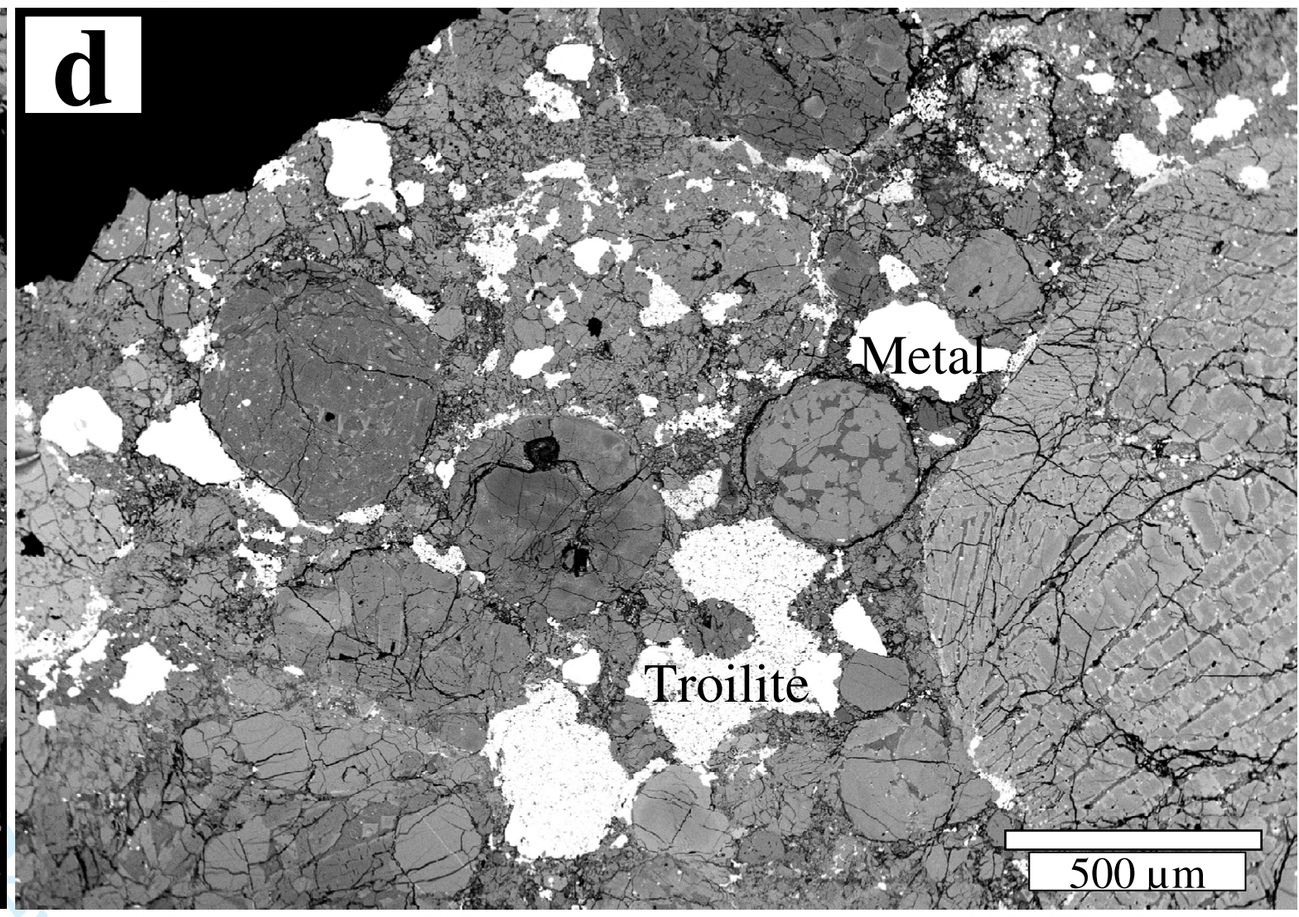
d
Metal
Troilite
500 µm

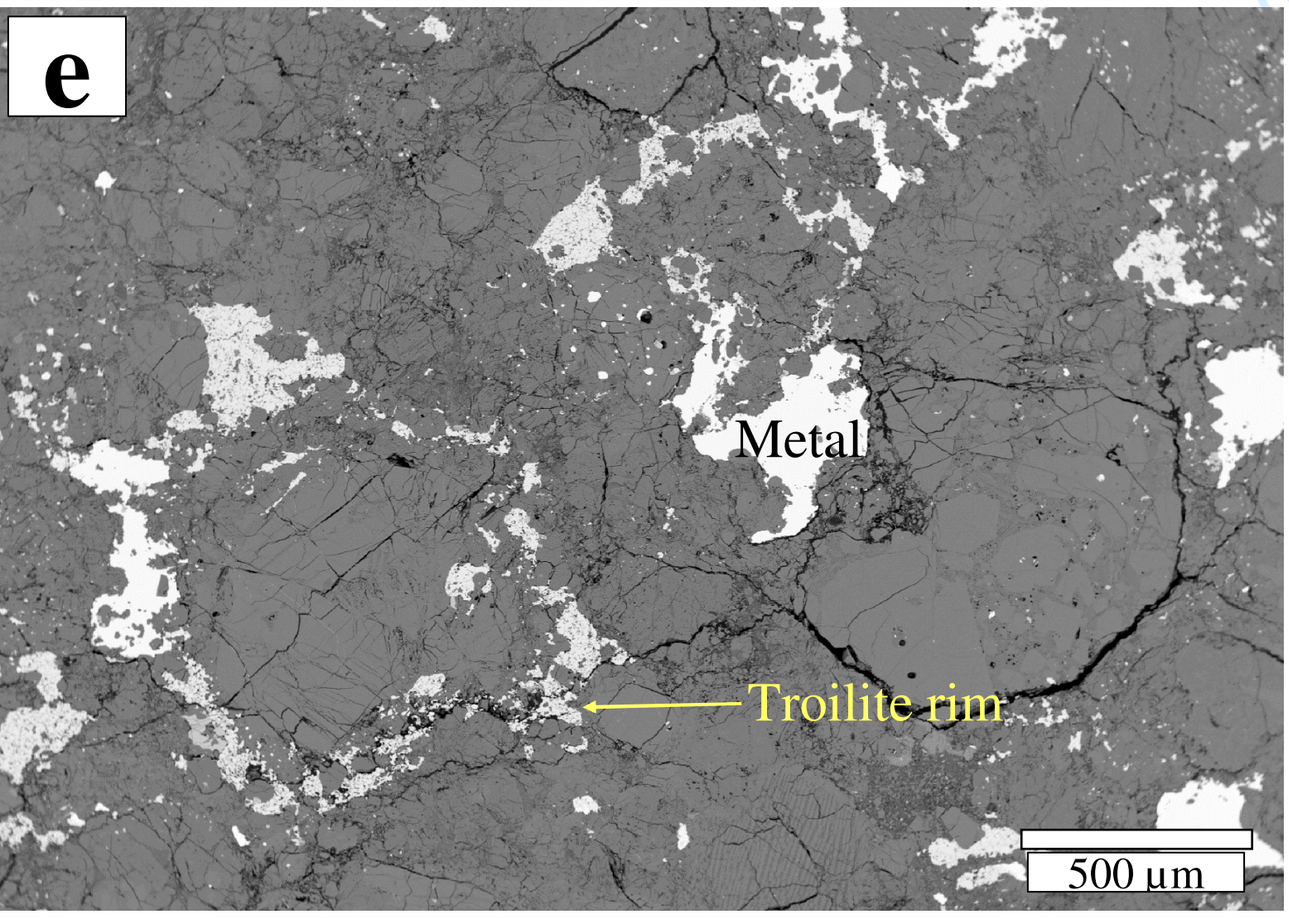
e
Metal
Troilite rim
500 µm

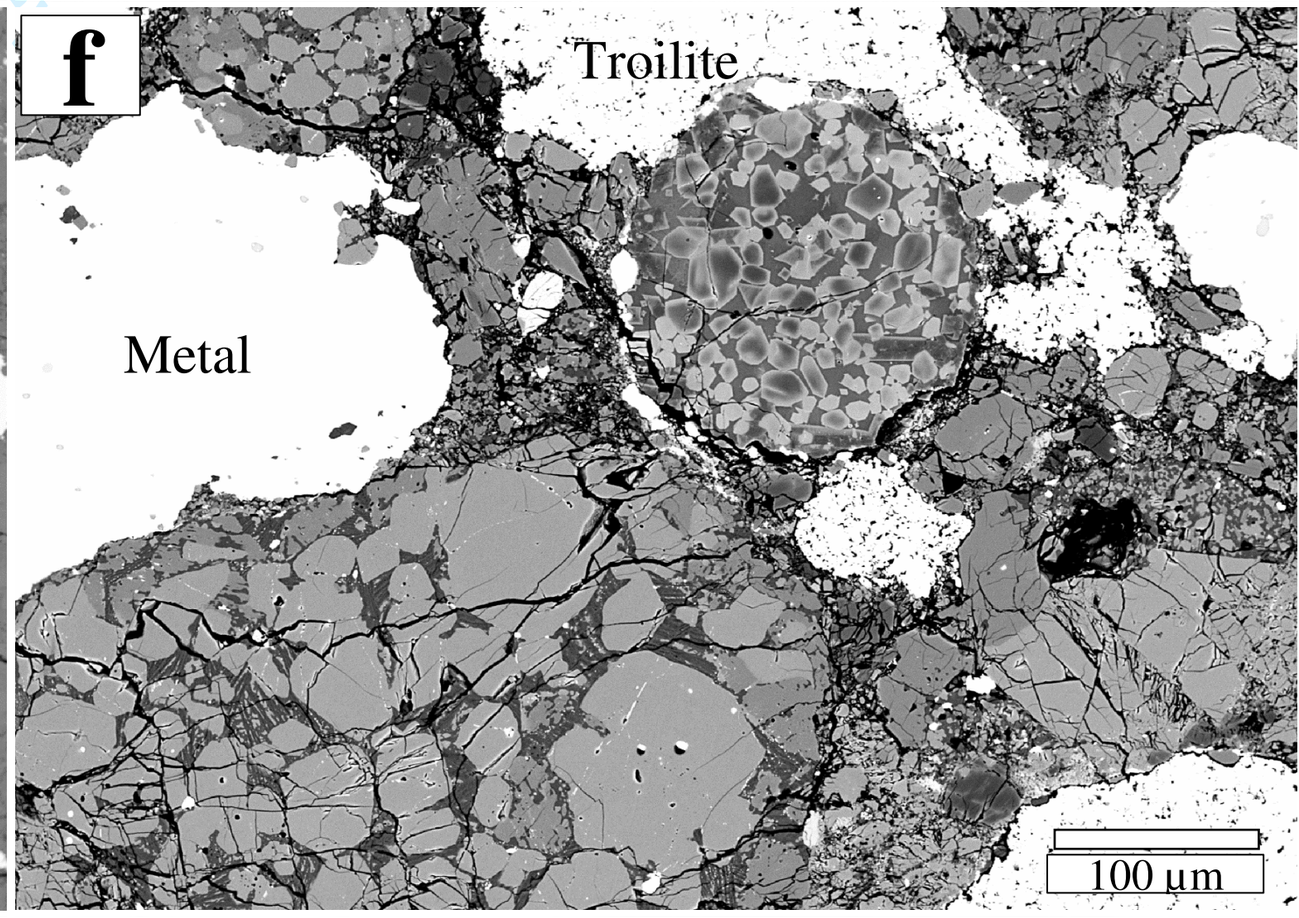
f
Troilite
Metal
100 µm

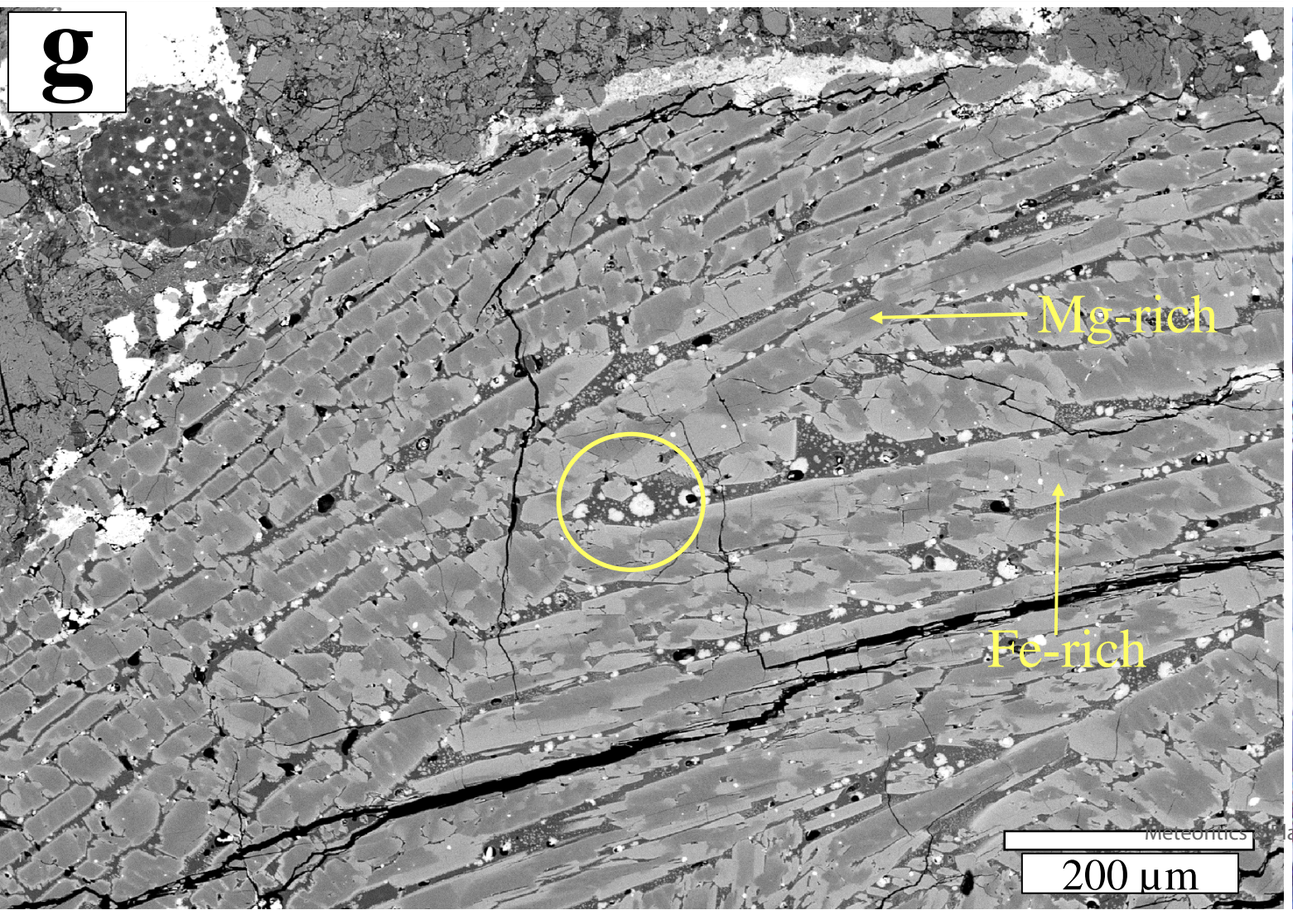
g
Mg-rich
Fe-rich
200 µm

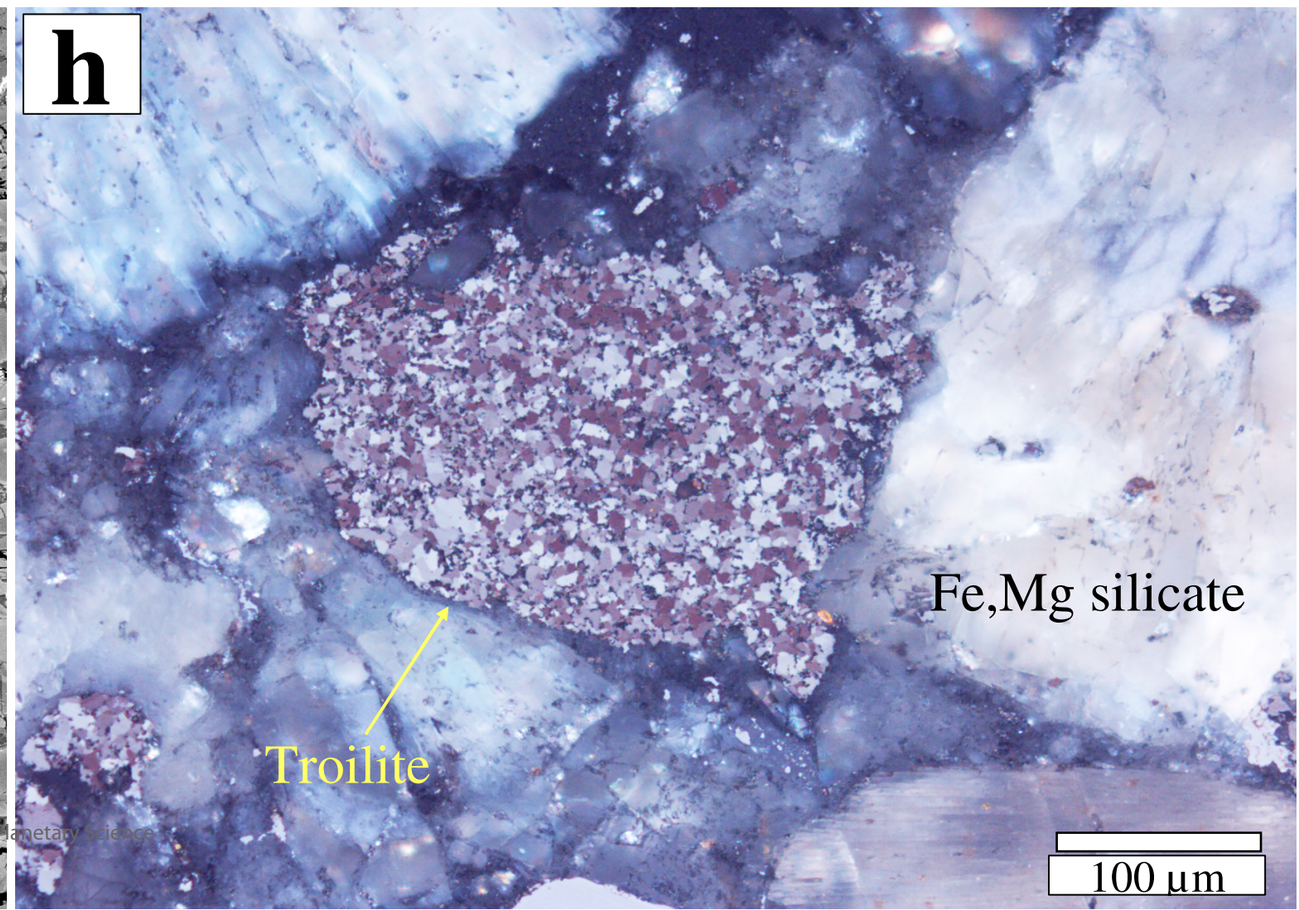
h
Troilite
Fe,Mg silicate
100 µm

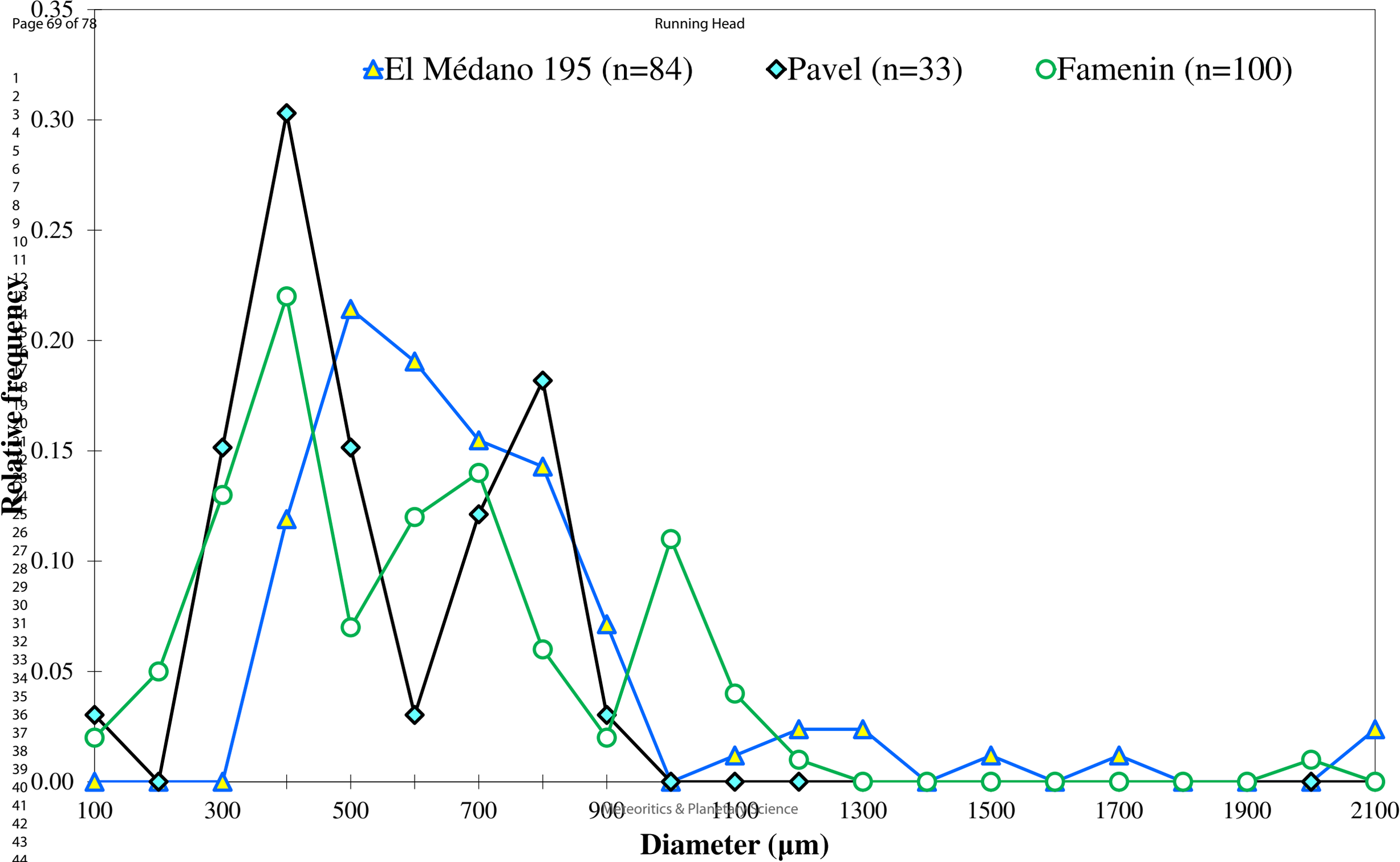
El Médano 195 (n=84)
Pavel (n=33)
Famenin (n=100)
Relative frequency
0.35
0.30
0.25
0.20
0.15
0.10
0.05
0.00
100
300
500
700
900
1100
1300
1500
1700
1900
2100
Diameter (µm)

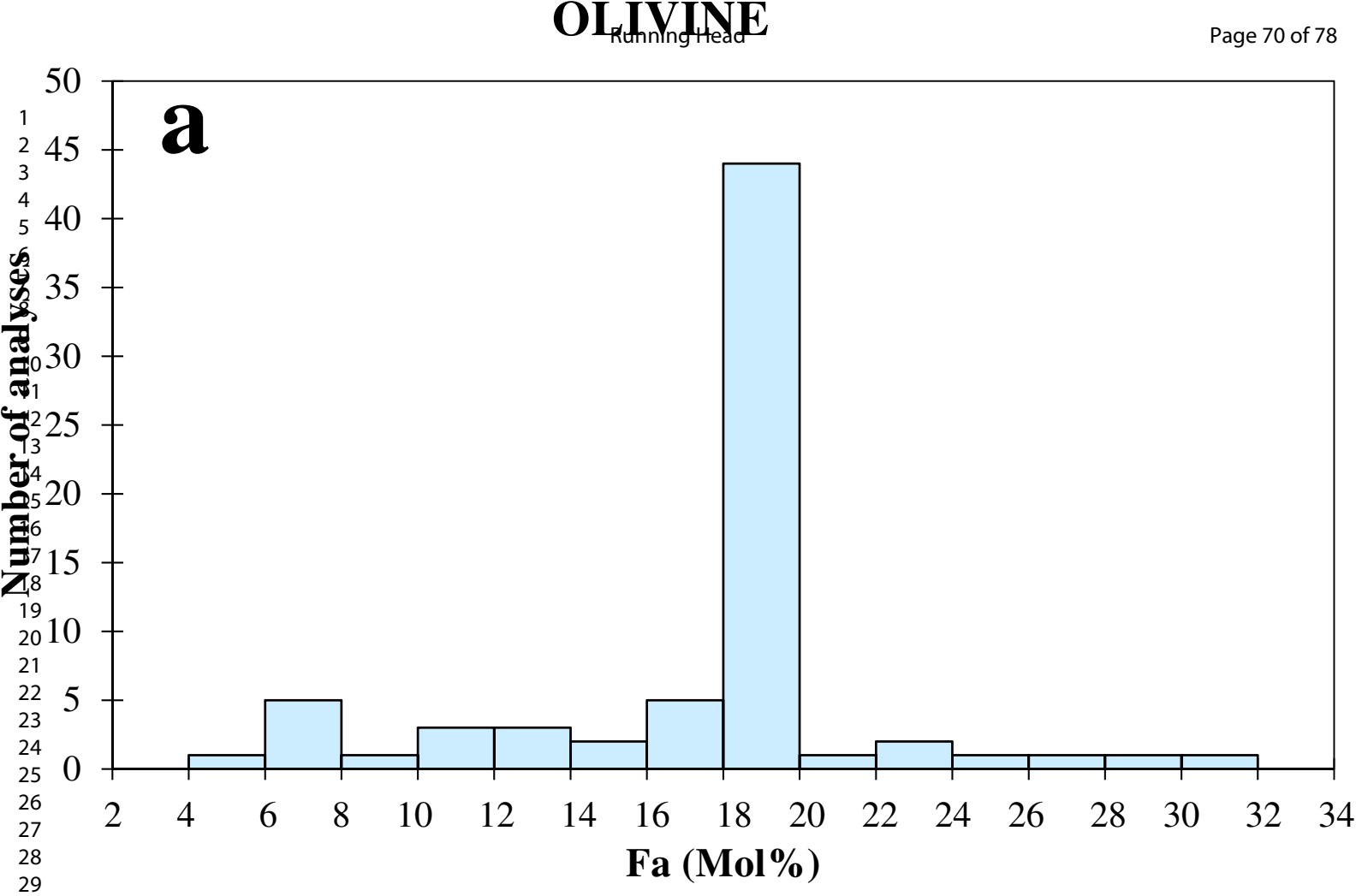
OLIVINE
a
Number of analyses
0
5
10
15
20
25
30
35
40
45
50
2
4
6
8
10
12
14
16
18
20
22
24
26
28
30
32
34
Fa (Mol%)

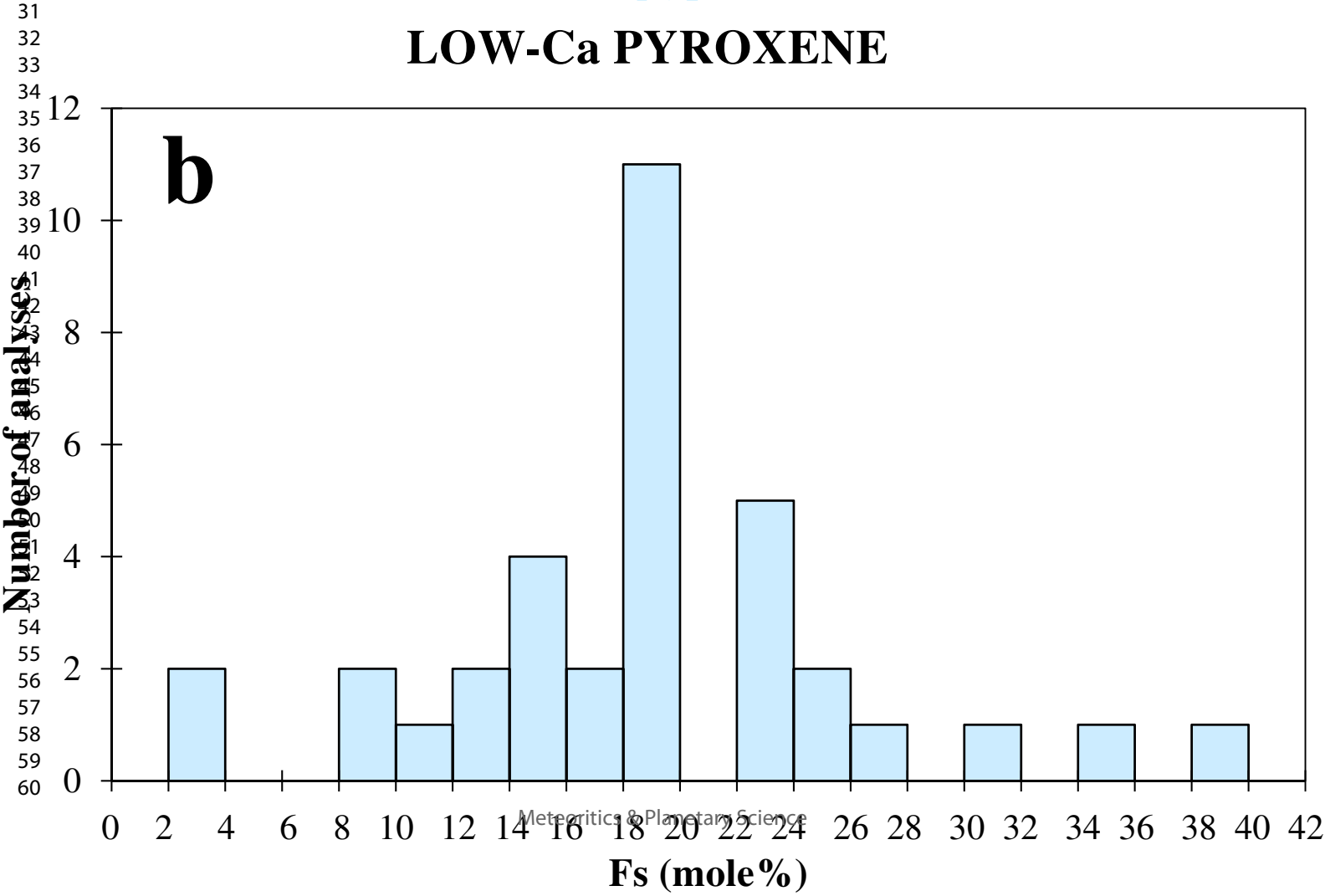
LOW-Ca PYROXENE
b
Number of analyses
0
2
4
6
8
10
12
0
2
4
6
8
10
12
14
16
18
20
22
24
26
28
30
32
34
36
38
40
42
Fs (mole%)

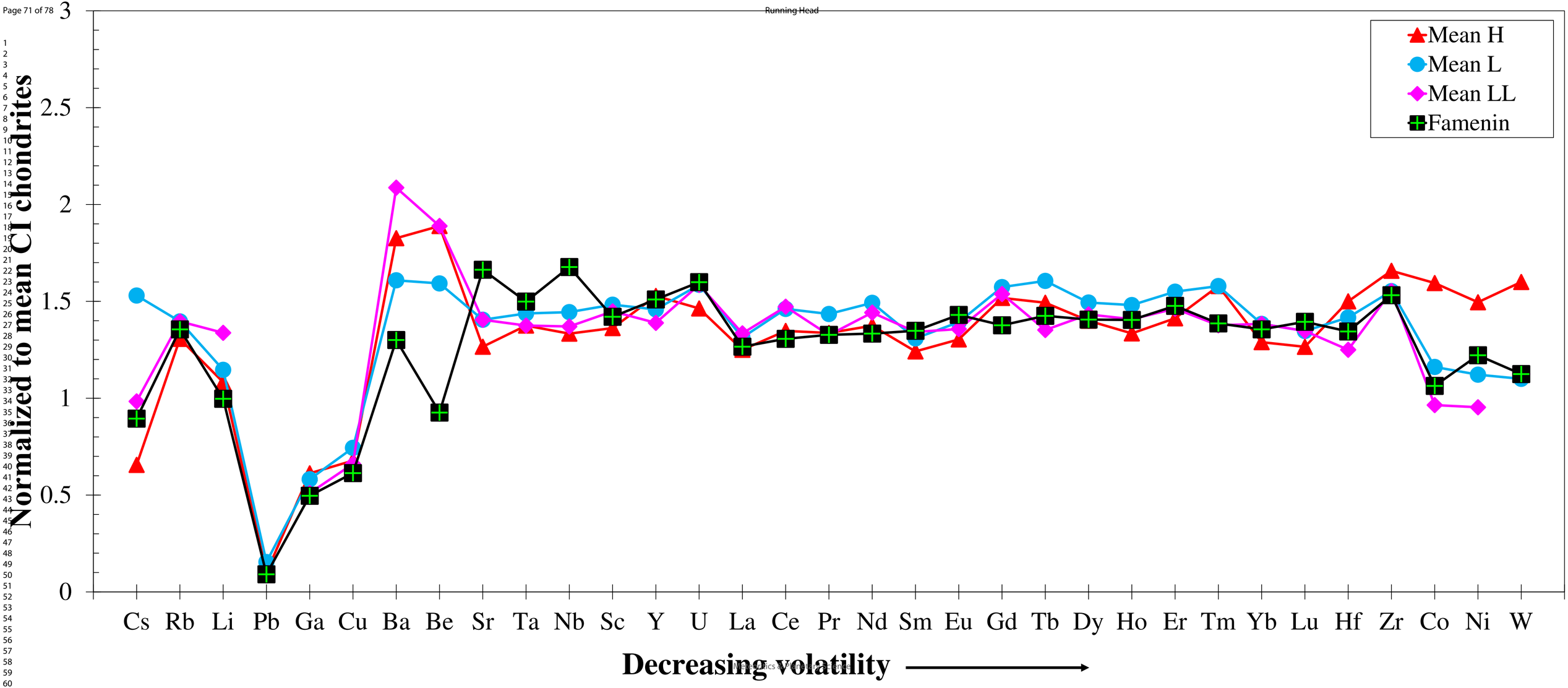
Mean H
Mean L
Mean LL
Famenin
Normalized to mean CI chondrites
3
2.5
2
1.5
1
0.5
0
Cs Rb Li Pb Ga Cu Ba Be Sr Ta Nb Sc Y U La Ce Pr Nd Sm Eu Gd Tb Dy Ho Er Tm Yb Lu Hf Zr Co Ni W
Decreasing volatility

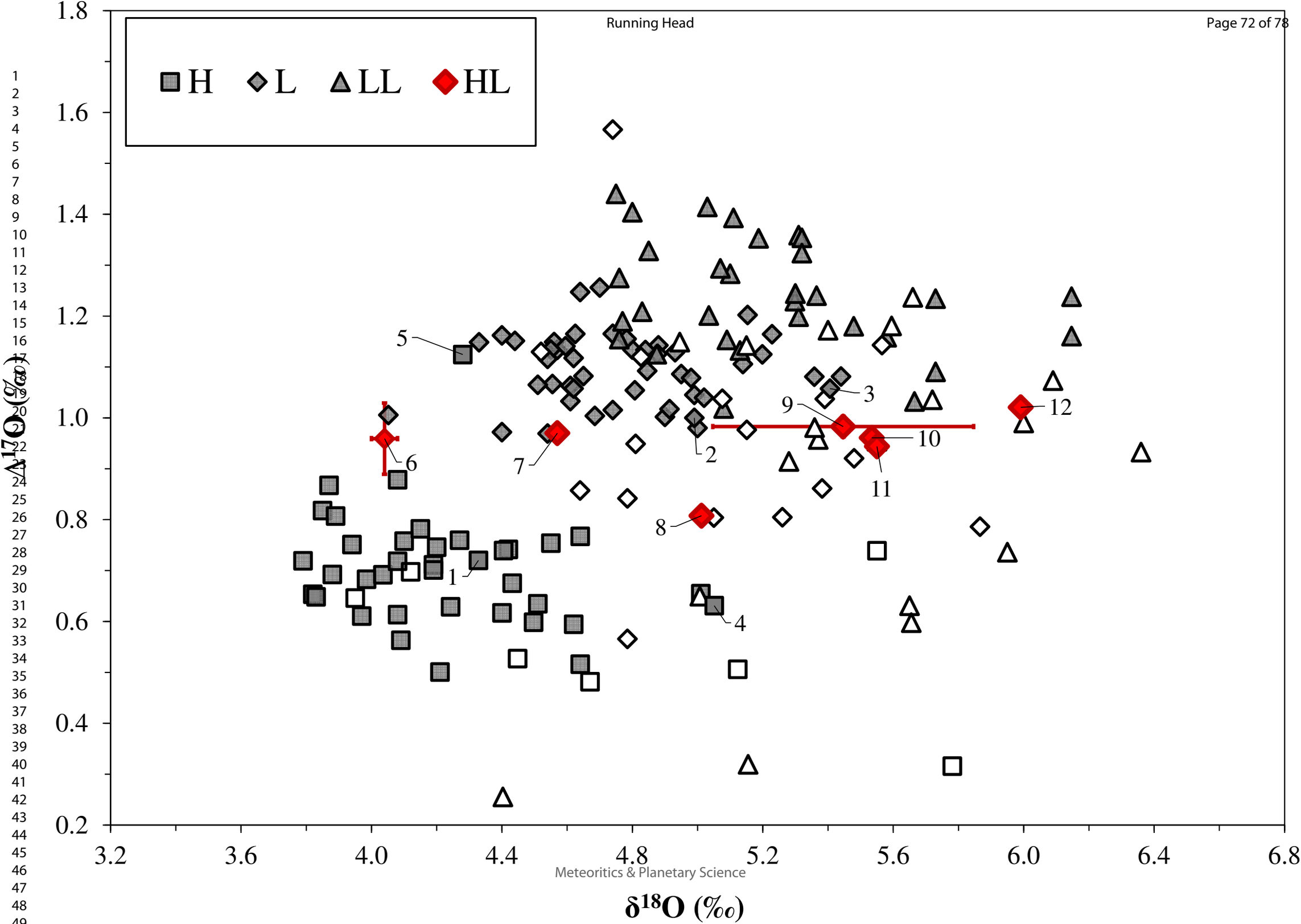
H
L
LL
HL
1.8
1.6
1.4
1.2
1.0
0.8
0.6
0.4
0.2
3.2
3.6
4.0
4.4
4.8
5.2
5.6
6.0
6.4
6.8
Δ17O (‰)
δ18O (‰)
1
2
3
4
5
6
7
8
9
10
11
12

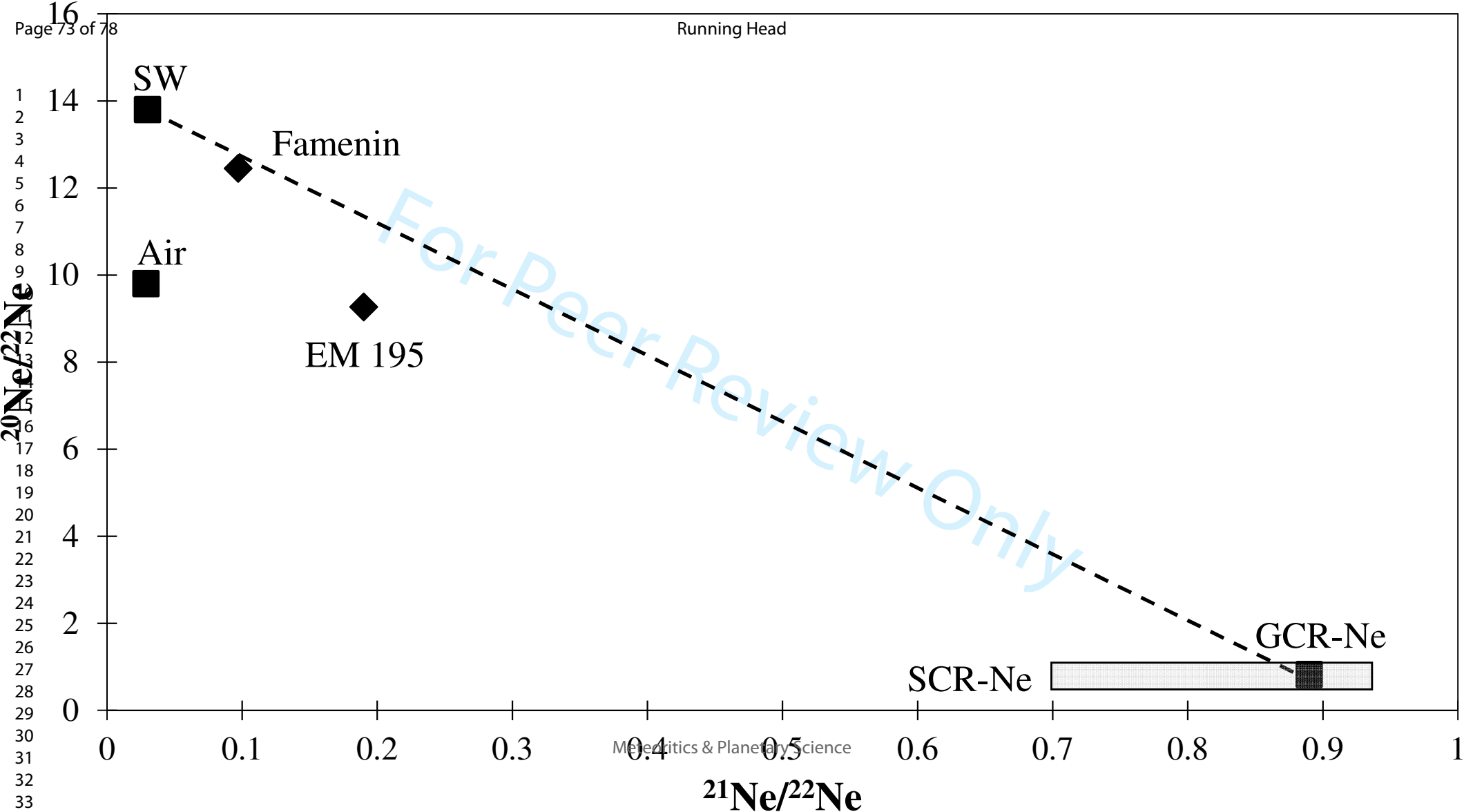

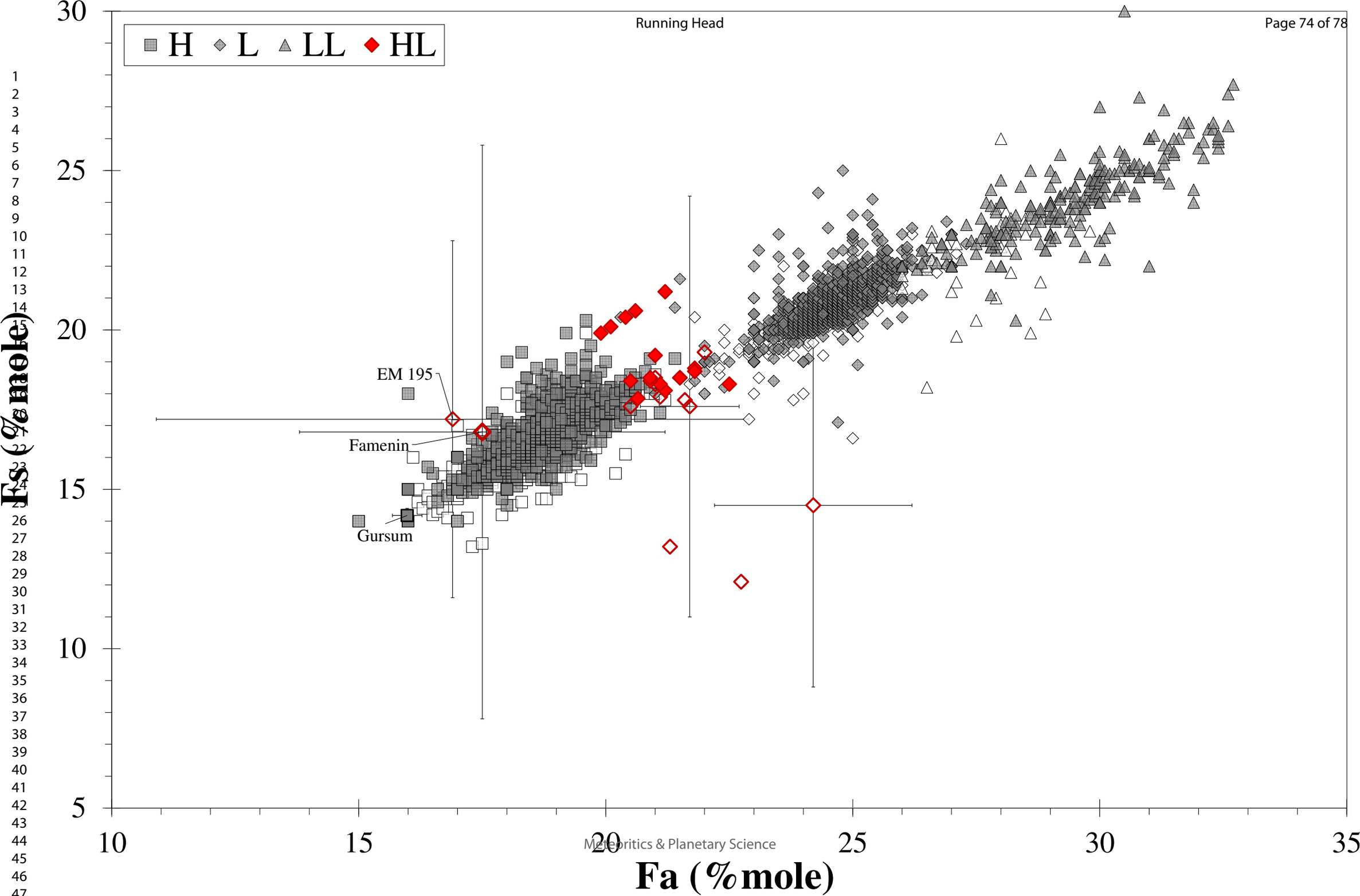
H
L
LL
HL
EM 195
Famenin
Gursum
Fs (%mole)
Fa (%mole)
30
25
20
15
10
5
10
15
20
25
30
35

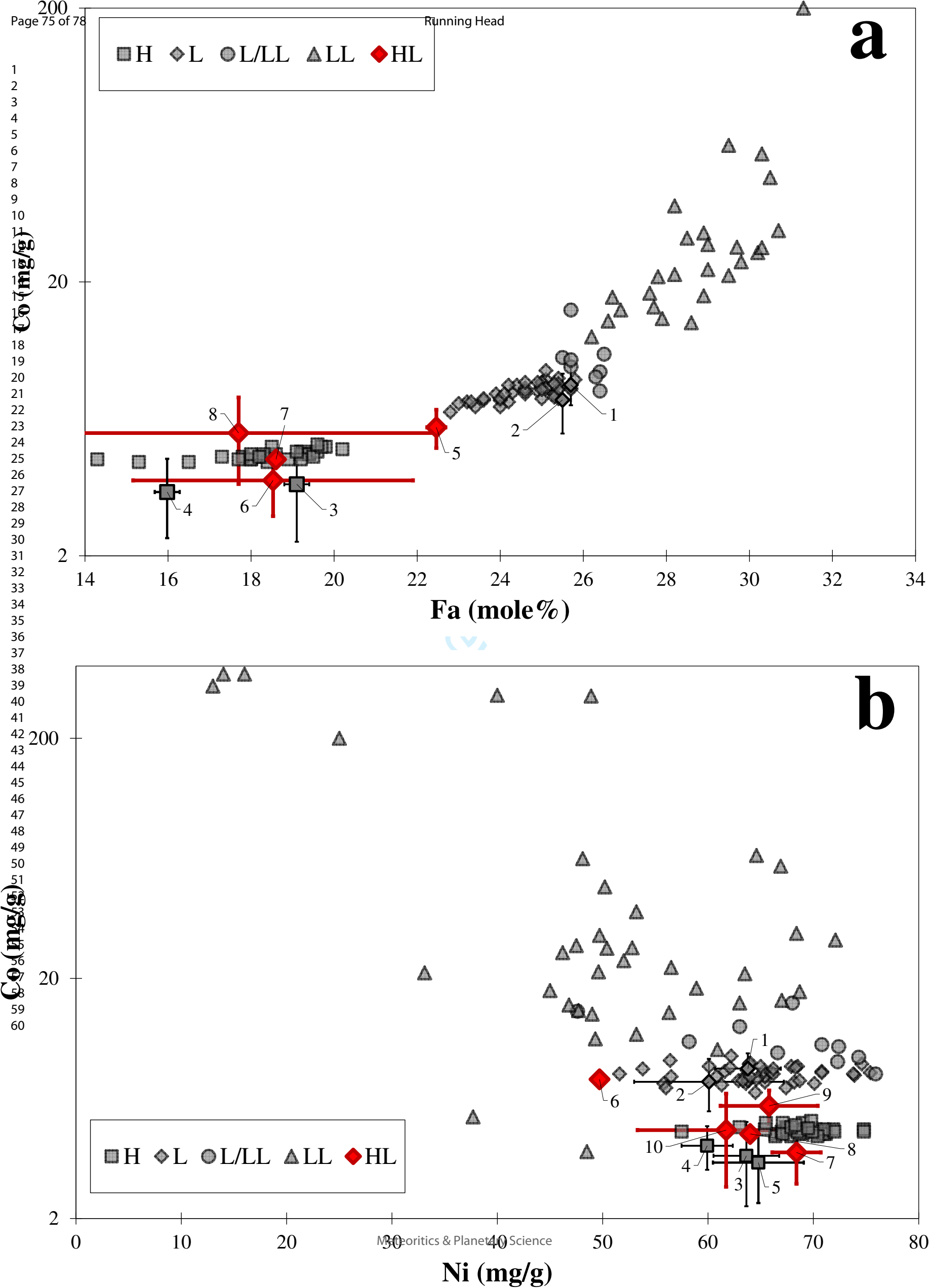
a
H
L
L/LL
LL
HL
200
20
2
Co (mg/g)
14
16
18
20
22
24
26
28
30
32
34
Fa (mole%)
1
2
3
4
5
6
7
8
b
200
20
2
Co (mg/g)
0
10
20
30
40
50
60
70
80
Ni (mg/g)
H
L
L/LL
LL
HL
1
2
3
4
5
6
7
8
9
10

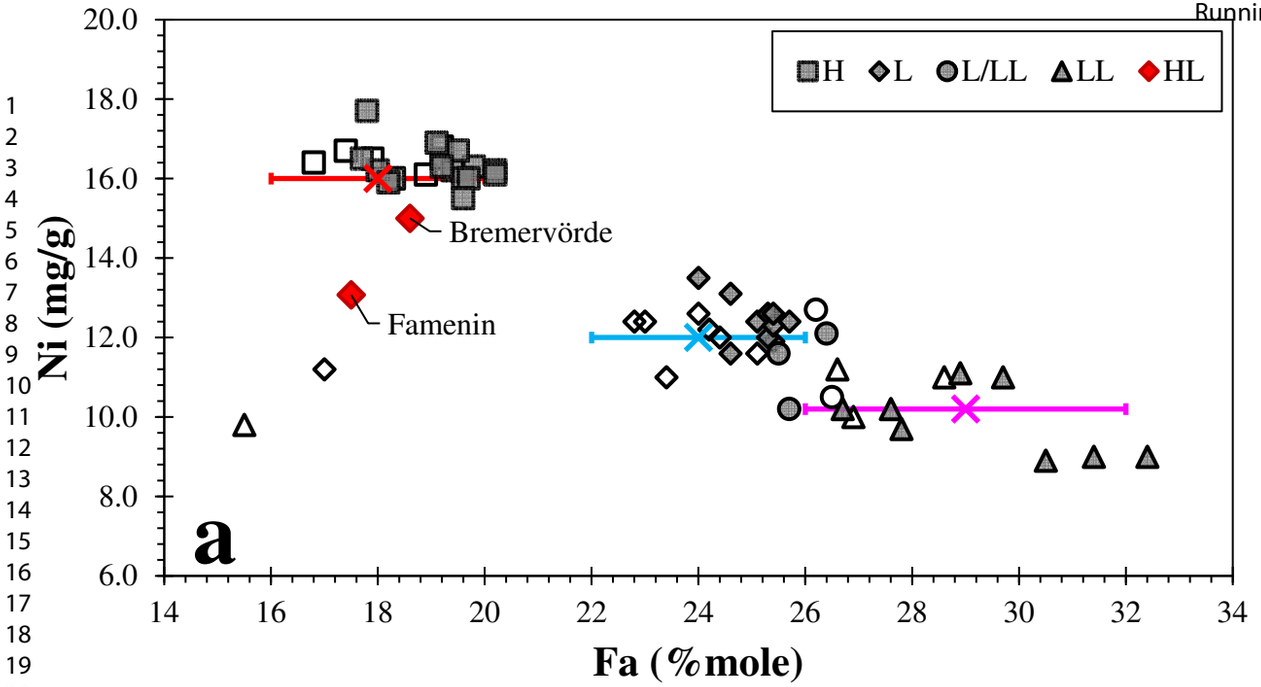
H
L
L/LL
LL
HL
Bremervörde
Famenin
Ni (mg/g)
Fa (%mole)
a

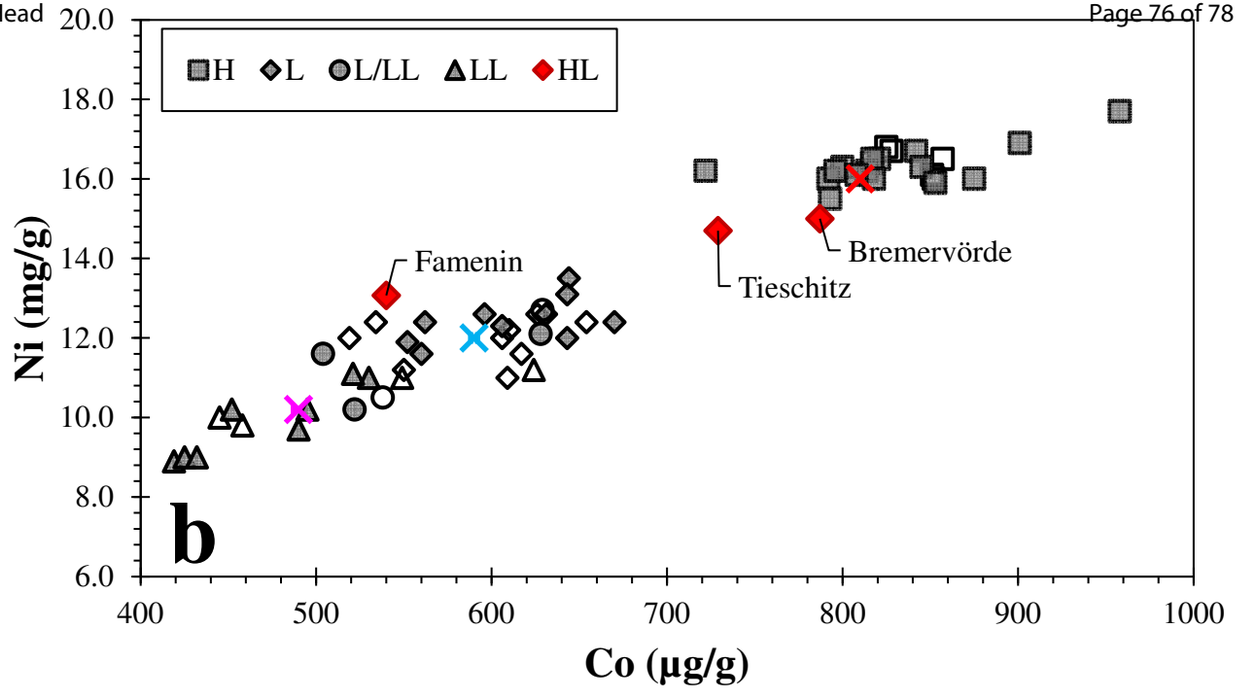
H
L
L/LL
LL
HL
Famenin
Tieschitz
Bremervörde
Ni (mg/g)
Co (µg/g)
b

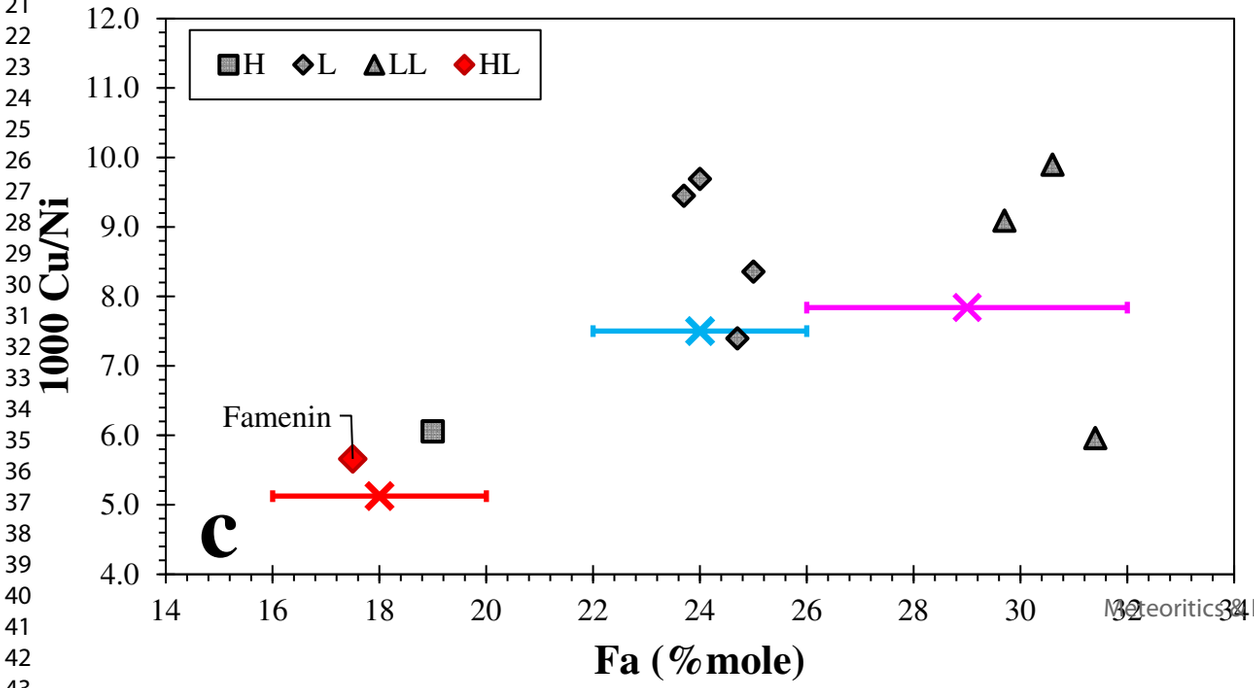
H
L
LL
HL
Famenin
1000 Cu/Ni
Fa (%mole)
c

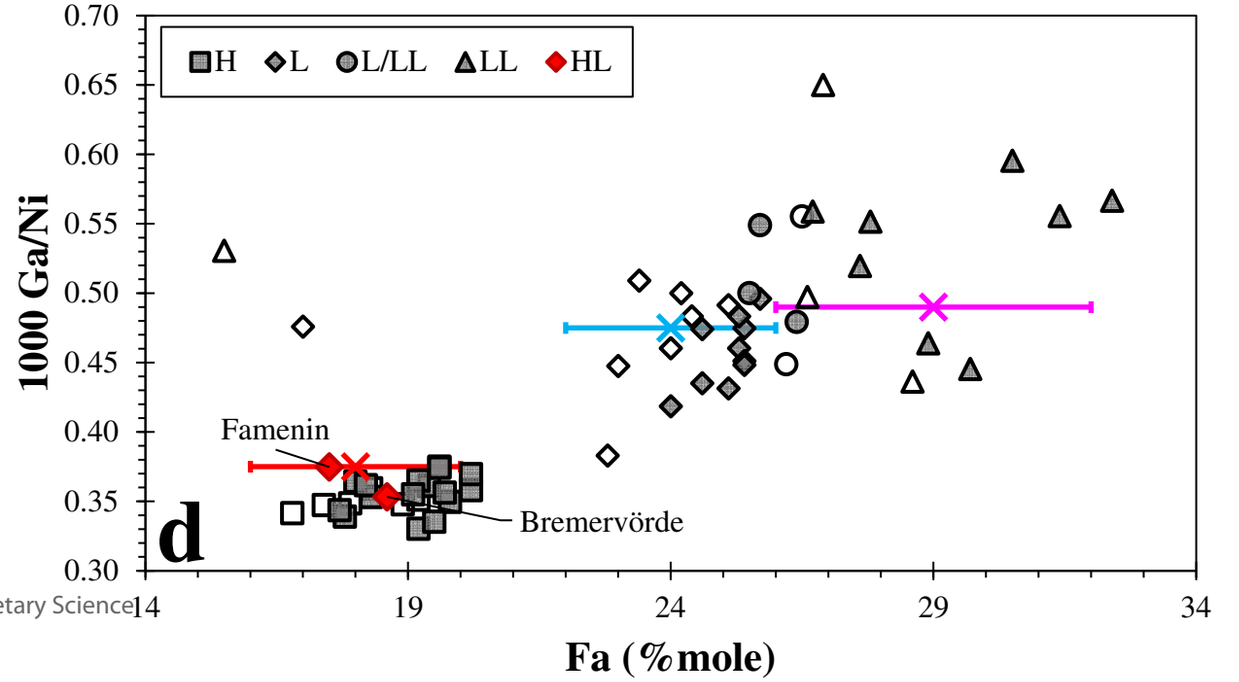
H
L
L/LL
LL
HL
Famenin
Bremervörde
1000 Ga/Ni
Fa (%mole)
d

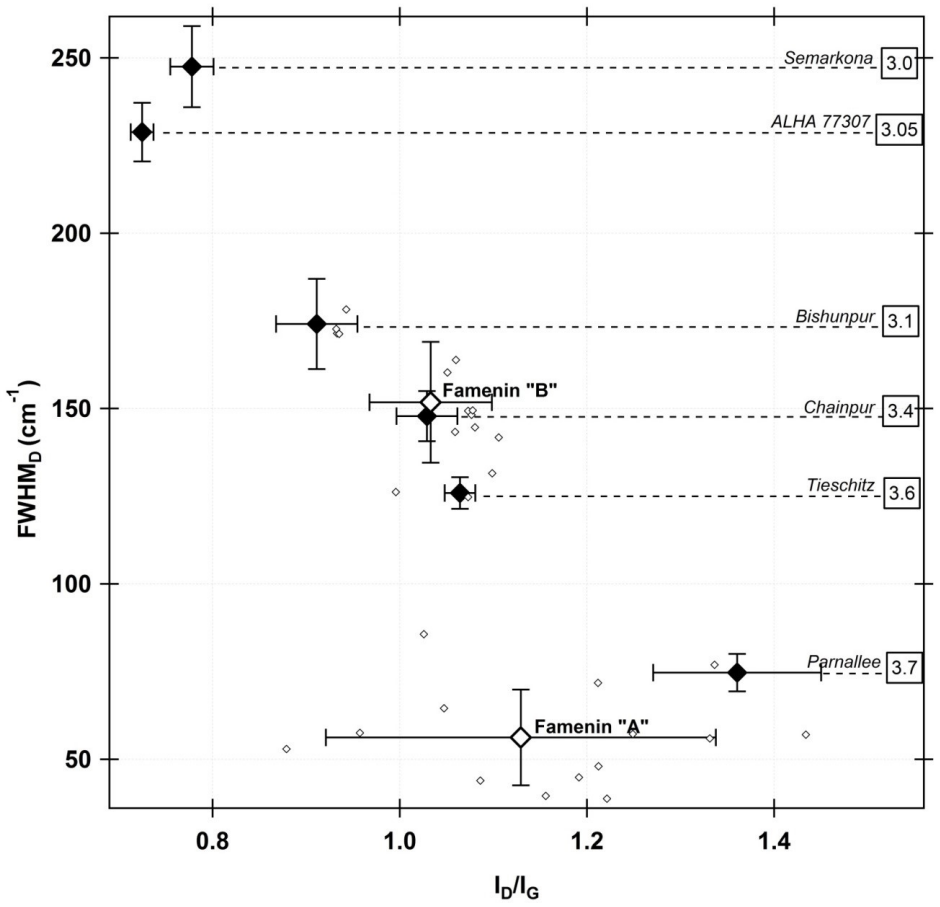

Fig. 12: Spectral parameters of Raman bands of carbonaceous materials in Famenin and in reference chondrites: FWHMD vs. ID/IG. Averages (points) and standard deviations (bars) are plotted for reference samples (black symbols) and for Famenin (open symbols). Spectral parameters of individual spectrum are plotted for Famenin (small grey diamonds). Reference chondrites data from Bonal et al. (2016).

160x144mm (220 x 220 DPI)

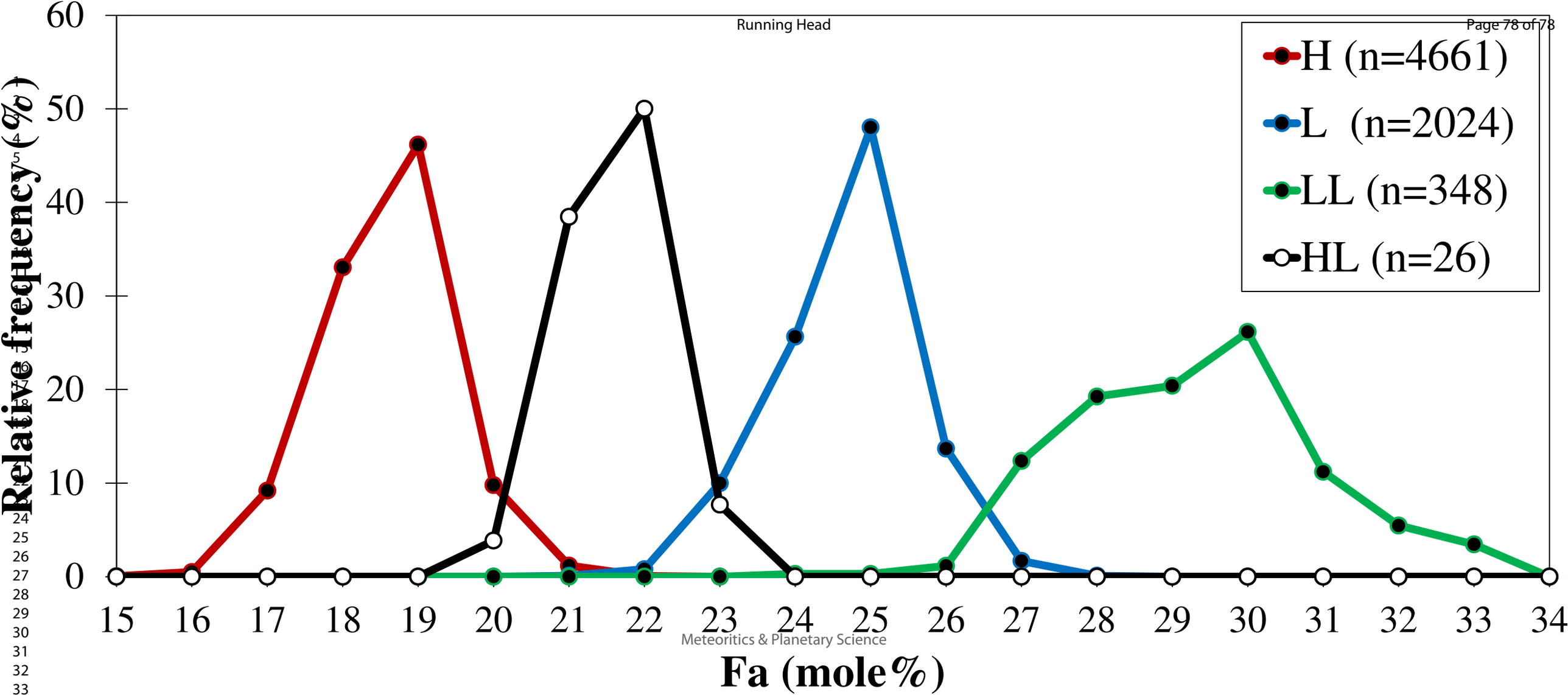
H (n=4661)
L (n=2024)
LL (n=348)
HL (n=26)
Relative frequency (%)
Fa (mole%)
0
10
20
30
40
50
60
15
16
17
18
19
20
21
22
23
24
25
26
27
28
29
30
31
32
33
34